REPUBLIC OF AZERBAIJAN

On the rights of the manuscript

ABSTRACT

of the dissertation for the degree of Doctor of Science

PHYSICO-CHEMICAL BASES FOR OBTAINING COPPER AND SILVER CHALCOGENIDES WITH p^3-ELEMENTS AND FUNCTIONAL PHASES BASED ON THEM

Specialty:	2303.01 – Inorganic Chemistry
Field of science:	Chemistry

Applicant: **Leyla Farhad Mashadiyeva**

Baku – 2025

The dissertation was carried out in the "Thermodynamics of functional inorganic compounds" laboratory of the Institute of Catalysis and Inorganic Chemistry named after acad. M.Nagiyev of the Ministry of Science and Education of the Republic of Azerbaijan

Scientific consultant: Corr.-member of ANAS, doctor of chemical sciences, professor
Mahammad Baba Babanly

Official opponents: Academician, doctor of chemical sciences, professor
Adil Abdulkhalyg Garibov

Corr.-member of ANAS, doctor of chemical sciences, professor
Tofig Abbasali Aliyev

Doctor of chemical sciences, professor
Ozbek Misirkhan Aliyev

Doctor of chemical sciences, professor
Mikola Volodimirovich Moroz

Dissertation council ED1.15 of the Supreme Attestation Commission under the President of the Republic of Azerbaijan operating at the Institute of Catalysis and Inorganic Chemistry named after acad. M.Naghiyev of the Ministry of Science and Education of the Republic of Azerbaijan

Chairman of the Dissertation council: Doctor of chemical sciences, academician
Dilgam Babir Taghiyev

Scientific secretary of the Dissertation council: Doctor of Phylosophy in Chemistry, dosent
Ulviyya Akhmed Mammadova

Chairman of the scientific seminar
Doctor of chemical sciences, professor
Akif Shikhan Aliyev

GENERAL DESCRIPTION OF WORK

Relevance and degree of investigation of the topic. The ongoing search, research, and application of new functional materials with unique properties is essential for scientific and technological progress. Due to their diverse physical and physicochemical properties, metal chalcogenides are used or considered promising materials in various high-tech fields.

In recent decades, copper- and silver-based chalcogenides have attracted particular attention from the scientific community due to their environmental safety, availability, and promising functional characteristics[1][2]. Many of these compounds combine electronic properties with high ionic conductivity, making them promising candidates for use in solid-state electrodes, selective membranes, sensors, and other devices. Among promising classes of functional materials, synthetic analogs of natural copper and silver chalcogenide minerals are of particular interest[3]. These compounds are of interest for the development of multifunctional systems with ionic and electronic conductivity, as well as functional materials in thermoelectric, photovoltaic, photocatalytic, and optical technologies. According to recent studies, some copper- and silver-containing chalcogenides also hold promise for biomedical applications.

In addition, many of them occur in nature as minerals, playing an important role in the geochemical processes of the lithosphere and being of interest for the geochemistry of the Earth[4].

---

[1] Coughlan, C. Compound Copper Chalcogenide Nanocrystals / C. Coughlan, M. Ibáñez, O. Dobrozhan, [etc] // Chem. Rev. - 2017, 117 (9), - p. 5865–6109

[2] Palchoudhury, S. Multinary copper-based chalcogenide nanocrystal systems from the perspective of device applications / S. Palchoudhury, K. Ramasamy, A. Gupta // Nanoscale Adv., - 2020, 2(8), - p. 3069-3082

[3] Babanly, M.B. Phase Diagrams in the Development of the Argyrodite Family Compounds and Solid Solutions Based on Them / M.B. Babanly, Y.A.Yusibov, S.Z. Imamaliyeva, [etc] // J. Phase Equilib. Diffus.,- 2024, 45, p.228–255

[4] Zhou, S. Tennantite and Enargite Rejection in the Copper Flotation—A Mini-Review / S. Zhou, T. Li, C. Wang, [etc] // Journal of Minerals and Materials Characterization and Engineering, - 2023. (11), - p. 63-68

An analysis of data from a number of studies on complex copper and silver chalcogenides demonstrates the potential for significantly improving their functional properties by manipulating their structure and chemical composition. Of particular interest in this context is the concept of entropy engineering, which entails the thermodynamic stabilization of functionally significant phases through increased compositional complexity and structural disorder.

Solving key problems in modern materials science, particularly in the field of alloy systems such as chalcogenides, relies heavily on physicochemical analysis as a fundamental method for studying phase equilibria and phase transformations[5]. In the early stages of materials development, physicochemical analysis enables the construction of phase diagrams of multicomponent systems, the identification of new compounds, and the determination of their thermal stability, crystallization regions, and phase transitions, which form the basis for selecting conditions for crystal synthesis and growth.

The use of physicochemical analysis methods has also demonstrated high efficiency in the design of existing materials and the optimization of their functional characteristics. This approach relies on the fundamental "composition-structure-property" relationship and enables the control of material properties. In complex systems containing analogous compounds, the formation of solid solutions of various types is possible, opening the way to targeted variation of composition and structure to improve functional properties.

Optimization of technological processes requires in-depth thermodynamic analysis and calculations, the effectiveness of which depends on the accuracy of the thermodynamic properties of substances. This underscores the relevance of systematic studies of phase equilibria and the thermodynamic properties of ternary and more complex chalcogenide systems, particularly those based on copper and silver.

[5] Saka, H., Introduction to Phase Diagrams In Materials Science and Engineering, World Scientific Publishing Company, 2020, p. 188

The Cu-As-X, Cu-Sb-X, Ag-As-X, and Ag-Sb-X (X = S, Se) systems are of particular interest for two reasons. First, their ternary compounds and glassy alloys are valuable functional materials with semiconducting, photovoltaic, optical, and other properties of practical importance. Second, many known ternary compounds of these systems occur naturally as minerals and are of interest both for fundamental research and for potential practical applications.

An analysis of the literature on phase equilibria in the above-mentioned systems and the properties of the ternary phases formed within them reveals that, despite the extensive study of several polythermal sections, complete phase equilibria have yet to be obtained. Known schematic projections of liquidus surfaces have serious shortcomings: the primary crystallization fields of most phases are arbitrarily delineated, isotherms are not shown, the precise coordinates of invariant equilibrium points are not determined, etc. Furthermore, data from existing studies on the Cu_2X-As_2X_3 and Cu_2X-Sb_2X_3 sections differ significantly in the number, composition, nature, and melting temperatures of the ternary compounds.

The above shows the importance of a detailed, comprehensive study of phase equilibria and thermodynamic properties of ternary chalcogenide systems of copper (silver) with arsenic and antimony.

In recent years, considerable attention has also been paid to the production of multicomponent chalcogenide phases in the quaternary systems Ag–A^{IV}–B^{V}–Se(Te) (where A^{IV} is Ge, Sn, Pb; B^{V} is Sb, Bi), in particular to compounds of the LAST (Lead–Antimony–Silver–Tellurium) and TAGS (Tellurium–Antimony–Germanium–Silver) types, as well as to the development of composite materials based on them and the study of their thermoelectric properties. An analysis of literary sources indicates that the composition of these materials is localized near the Ag_2Te–$A^{IV}Te$–$B^{V}{}_2Te_3$ concentration planes of the corresponding systems. In this regard, a targeted search for these phases and composites, as well as the optimization of their composition and functional characteristics, requires a comprehensive study of phase equilibria, thermodynamic and crystallographic properties of intermediate compounds within the specified concentration ranges.

A rational solution to research problems is ensured by the integrated application of experimental methods of physicochemical analysis and the electromotive force (EMF) method, which is one of the most accurate equilibrium methods of chemical thermodynamics and allows for the simultaneous study of phase equilibria and thermodynamic properties of systems.

Object and subject of research. Based on the above, the objects of study were the ternary systems Cu-As-S(Se), Cu-Sb-S, Ag-As-S(Se), and Ag-Sb-Se, as well as some quasi-ternary systems including silver (copper) chalcogenides with heavy p^2- and p^3-elements. The subject of the study was a physicochemical and thermodynamic investigation of these systems.

The purpose and objectives of the study. The primary objective of this dissertation was to develop physicochemical foundations for the production of copper (silver) chalcogenides with heavy p^3-elements, as well as complex phases with controlled composition and properties based on these elements, based on the results of comprehensive studies of phase equilibria and the thermodynamic properties of the corresponding systems.

To achieve this goal, the **following tasks** were set and solved:

- setting up and conducting complex experimental studies that make it possible to obtain mutually consistent data on phase equilibria and thermodynamic characteristics of many ternary A^I-B^V-X, quasi-ternary Ag_2X-A^{IV}-$B^V{}_2X_3$, and quaternary systems Cu-Ge-Sb-X (A^I - Cu, Ag; A^{IV} - Sn, Pb; B^V - As, Sb, Bi; X – S, Se, Te);
- obtaining reliable pictures of phase equilibria in the studied systems, identifying intermediate compounds and phases of variable composition, determining their areas of primary crystallization and homogeneity, obtaining them in a single-phase state, and characterizing them;
- selection of the most appropriate modifications of the electromotive force method to ensure the interrelationship between thermodynamic studies and data on solid-phase equilibria in the systems under study, and the calculation of partial and integral thermodynamic functions of the phases;
- generalization of the obtained sets of experimental data,

identification of patterns of phase formation and phase equilibria in the systems under study.

Research Methods. The studies were conducted using differential thermal analysis (DTA), X-ray diffraction (XRD), scanning electron microscopy (SEM), microhardness measurements, and two modifications of the EMF method -with a solid Cu^+ (Ag^+) conducting electrolyte and a liquid glycerol electrolyte. Two types of concentration cells were used for each modification (see Chapter 5).

DTA was performed in evacuated ampoules on NETZSCH DSC 500 Pegasus and Linseis STA PT 1600 differential scanning calorimeters, on a Thermoscan-2 device, and on a multichannel DTA setup assembled around the TC-08 Thermocouple Data Logger electronic data recorder. Phase transformation temperatures were measured using chromel-alumel and platinum-platinum-rhodium thermocouples. Powder X-ray diffraction patterns of the alloys were recorded on Bruker D2 Phaser and D8 ADVANCE diffractometers using CuKα radiation. SEM images were recorded on JEOL JSM-7600F and Tescan Vega 3 Field Emission Scanning Electron Microscopes.

Provisions submitted for defense:

1. New phase equilibria obtained in the studied ternary and quaternary systems – projections of liquidus surfaces, a series of polythermal and isothermal sections of T-x-y phase diagrams.
2. Types and coordinates of non- and monovariant equilibria, primary crystallization fields and phase homogeneity regions, crystallographic data for the new phases obtained.
3. New thermodynamic data sets – relative partial molar functions, standard thermodynamic formation functions, and standard entropies for 22 copper (silver) chalcogenides with arsenic (antimony), and more than 20 solid solution compositions of the $A^{IV}X$-$AgB^{V}X_2$ systems.
4. Identified features of phase formation and phase equilibria in the studied systems.

Scientific Novelty. The following new scientific results were obtained in the work, which form the physicochemical basis for producing copper and silver chalcogenides with heavy p^3-elements

and complex phases of variable composition based on them:

- new phase equilibria in the Cu-As-S(Se) and Cu-Sb-S systems, significantly different from those available in the scientific literature, were obtained. These include projections of the liquidus surfaces and some isothermal and polythermal sections of their T-x-y diagrams. In particular, in contrast to existing data, instability of the Cu_2S-As_2S_3 and Cu_2S-Sb_2S_3 sections of the corresponding ternary systems was demonstrated. Experimental data confirming this result were presented and discussed in detail;

- it was shown that 14 equilibrium thermodynamically stable ternary compounds exist in these ternary systems. The remaining ternary compounds mentioned in the literature were characterized as metastable phases, absent from the equilibrium phase diagrams;

- the character of phase equilibria in the Ag_2Te-$SnTe$-Sb_2Te_3, Ag_2Te-$SnTe$-Bi_2Te_3, Ag_2Se-$PbSe$-Sb_2Se_3, and Ag_2Te-$PbTe$-Sb_2Te_3 systems was established, and the projections of the liquidus surfaces and some vertical and horizontal sections of their bulk phase diagrams were constructed. It was shown that all these systems are quasi-ternary planes of the corresponding quaternary systems and are characterized by the formation of wide or continuous solid solutions along the $A^{IV}X$-$AgB^{V}X_2$ sections. Solid solutions of the given compositions were obtained in individual form, and their crystal parameters were determined;

- relative partial thermodynamic functions of copper and silver (concentration cells with a solid cation-conducting electrolyte), as well as quasi-components of PbSe, PbTe, and lead (concentration chains relative to PbSe and PbTe with a glycerol electrolyte) in alloys were calculated from EMF measurement data for two types of concentration chains;

- new, mutually consistent data sets were obtained for the standard thermodynamic functions of formation ($\Delta_f G°$, $\Delta_f H°$) and standard entropy ($S°$) for ternary sulfide and selenide compounds of copper (14 compounds) and silver (8 compounds), as well as for many quaternary phases of variable composition along the $A^{IV}X$-$AgB^{V}X_2$ sections;

- by generalizing the obtained sets of new results, some patterns of

phase formation and phase equilibria in the studied systems were revealed.

Theoretical and practical significance of the study. *The theoretical significance* of the study lies in the fact that the new, consistent data obtained on the phase equilibria, thermodynamic, and crystallochemical characteristics of the studied systems make a significant contribution to the development of the chemistry, thermodynamics, and materials science of functional materials based on complex copper and silver chalcogenides. *The practical significance* of the study lies in the formation of a scientific basis for the targeted production of new functional materials based on copper and silver chalcogenides. The obtained consistent data on the phase equilibria, thermodynamic, and crystallochemical characteristics of the studied systems enable a well-founded approach to the selection of synthesis conditions and the targeted growth of single crystals of phases with a given composition and properties. The developed approaches and identified patterns can be used in the creation of process regulations aimed at producing promising materials with energy conversion functions, ionic conductivity, and a number of other functional characteristics in demand in modern scientific and technical applications. These data are also fundamental characteristics of substances and can be included in relevant reference publications and information databases on inorganic substances and materials used in science-intensive technologies.

Selected results obtained during the dissertation research have been included in the databases of international scientific information agencies Springer, Elsevier, and Thomson Reuters.

As of June 1, 2025, according to Google Scholar Citations, the author's 19 scientific publications on the dissertation topic have received over 350 citations, demonstrating scientific interest in the topic and the results of the work.

Analysis of the literature on the initial binary and ternary compounds comprising the studied systems suggests that the resulting new multicomponent phases of variable composition possess potential as polyfunctional materials. These compounds and phases can combine mixed ionic-electronic conductivity, as well as

thermoelectric, photovoltaic, optical, and other functional properties. Further studies of their physicochemical characteristics will open up prospects for the practical application of these phases in high-tech areas of inorganic materials science.

The materials and results of this dissertation can also be used in the educational process for master's and doctoral students at the Republic's universities. Specifically, they provide a methodological and substantive basis for teaching specialized disciplines such as "Physicochemical Analysis," "Inorganic Materials Science," "Thermodynamics of Solutions," "Thermodynamics of Phase Equilibria," and other courses related to chemistry and solid-state physics.

Testing and application. The dissertation resulted in the publication of 52 scientific papers, including 25 articles, 24 of which were published in international journals indexed in the Web of Science and Scopus databases. Of these, 17 articles were published in journals included in the Science Citation Index Expanded (SCIE). *Three articles were review articles*, one of which was published in a journal indexed in the Web of Science (SCIE), and two in journals included in the Scopus database. One work was presented as a chapter in the book "Properties and Uses of Antimony," published by Nova Science Publishers-New York, which is indexed in the Book Citation Index (Web of Science Core Collection) and Scopus databases.

The results of the work were reported and discussed at the following scientific conferences:

1-я Всероссийская научная конференция XIV, XV и XVI всероссийские конференции "Высокочистые вещества и материалы. Получение, анализ применение" (Нижний Новгород, Россия, 2011; 2015; 2018); VI Украинский съезд по электрохимии (Днепропетровск, Украина, 2011); "Biokimyəvi nəzəriyyələrin aktual problemləri" 2-ci, 5-ci, 6-cı, 8-ci, 11-ci Beynəlxalq Konfranslar (Gəncə, Azərbaycan, 2011; 2018; 2019; 2021; 2024); II международная научно-техническая конференция "Функциональные и конструкционные материалы (Донецк, Украина, 2011); XII International conference on crystal chemistry of

intermetallic compounds (Lviv, Ukraine, 2013); XVI Российская конференция по физической химии и электрохимии расплавленных и твердых электролитов (Екатеринбург, Россия, 2013); V международная конференция «Современные методы в теоретической и экспериментальной электрохимии» (Плес, Россия, 2013); VII Всерос. Конф. "физико-химические процессы в конденсированных средах и на межфазных границах-ФАГРАН-2015" (Воронеж, Россия, 2015); Akademik T.N.Şaxtantinskinin 90 illik yubileyinə həsr olunmuş respublika elmi konfransı (Baki, Azərbaycan, 2015); 2nd and 3rd International Turkic World Conference on Chemical Sciences and Technologies (ITWCCST) (Skopje, Macedonia, 2016; Baku, Azərbaycan, 2017); XI международное Курнаковское совещание по физико-химическому анализу (Воронеж, 2016); 13-ое и 16-ое Совещания с международным участием "Фундаментальные проблемы ионики твердого тела" (Черноголовка, 2016; 2022); AMEA-nın akad.M.Nağıyev ad. Kataliz və Qeyri-üzvi Kimya İnstitutunun 80 illik yubileyinə həsr olunmuş elmi konfransı (Baki, Azərbaycan, 2016); Всероссийская конф. С межд. участием "Химия твердого тела и функциональные материалы" и XII всероссийский симпозиум с межд. участием "Термодинамика и материаловедение" (Санкт-Петербург, 2018); "XXII International Conference on Chemical Thermodynamics in Russia" (Saint Petersburg, Russia, 2019); 9th Rostocker International Conference “Technical Thermodynamics: Thermophysical Properties and Energy Systems” THERMAM-2020 (Rostock, Germany, 2020).

Name of the organization where the work was carried out. This dissertation was completed at the M. Nagiyev Institute of Catalysis and Inorganic Chemistry of the Ministry of Science and Education of the Republic of Azerbaijan.

Volume and structure of the work. The dissertation consists of an introduction (17921 characters), six chapters (Chapter I - 59530 characters; Chapter II - 60099 characters; Chapter III - 68331 characters; Chapter IV - 67554 characters; Chapter V - 56018 characters; Chapter VI - 23289 characters), main results and conclusions (4764 characters), a list of references and the author's

published works on the topic of the dissertation (471 titles). The dissertation is presented on 397 pages, of which 218 pages constitute the main text (a total of 347,506 characters), and it contains 162 figures and 58 tables.

Author's contribution. The author personally formulated the goal and objectives of this dissertation, ensuring a clear focus for the research and a logical sequence of the completed stages. The methodological approaches and experimental techniques used to solve the stated problems were developed and substantiated.

The author collected, processed, and comprehensively analyzed the experimental data, ensuring their reliability and completeness. A significant portion of the experimental studies, including the synthesis, phase equilibria, and thermodynamic and crystallochemical characteristics of copper- and silver-based chalcogenide systems, was performed directly by the author. Furthermore, the author actively participated in the interpretation of the obtained results, their systematization, and the preparation of scientific publications, and also presented papers at scientific conferences and seminars.

MAIN CONTENT OF THE WORK

The introduction substantiates the relevance of the dissertation topic and formulates the goal, objectives, scientific novelty, and theoretical and practical significance of the results obtained in the dissertation.

The first chapter briefly describes and critically analyzes the literature on T-x diagrams in $A^{I}(B^{V})$-X (A^{I}-Cu, Ag; B^{IV}-As, Sb; X-S, Se, Te) and the physicochemical properties of copper and silver chalcogenides; on phase equilibria in ternary A^{I}-B^{V}-X and quasi-ternary Ag_2X-$A^{IV}X$-$B^{V}{}_2X_3$ systems (A^{IV}-Sn, Pb; B^{V}-As, Sb, Bi; X-S, Se, Te) as well as the physicochemical and thermodynamic properties of their ternary compounds and phases.

At the end of the chapter, data on the state of knowledge of complex systems including copper (silver) chalcogenides with p3 elements are presented, and the choice of research objects is justified. A separate subsection (1.1) is devoted to new studies on the various

functional properties of copper and silver chalcogenides with p3 elements and materials based on them.

The second chapter is devoted to the methodological aspects of planning and organizing the interrelated study of phase equilibria and the thermodynamic properties of systems, methods for synthesizing compounds and alloys (Sections 2.1 and 2.2), and a brief description of the experimental research methods and associated instrumentation and setups (Section 2.3).

High-purity elemental components purchased from the German companies Alfa Aesar and Evochem were used in the syntheses.

Synthesis of the initial binary and ternary compounds was accomplished by direct alloying of the elementary components at temperatures above their melting points under vacuum conditions. This minimized oxidation and evaporation of volatile elements, as well as yielding samples uniform in composition and phase state. Alloys of the studied systems were prepared from previously synthesized and identified binary and ternary compounds in sealed quartz ampoules evacuated to ~10^{-2} Pa. To equalize the composition and establish an equilibrium structure, the resulting alloys were subsequently annealed at optimal temperatures. The synthesis and annealing conditions are described in the relevant sections of this dissertation.

To conduct the experiments in this work, traditional methods of physicochemical analysis (DTA, X-ray diffraction, SEM, microhardness measurements) and two modifications of the EMF method (concentration relative to the electrodes of galvanic cells with Cu^+ (Ag^+) conductive solid electrolytes ($Cu_4RbI_3Cl_2$ and Ag_4RbI_5) and with a glycerol electrolyte) were used. The corresponding devices and installations are described in Chapter 2 of the dissertation.

The third chapter presents the results of an experimental study of phase equilibria in the ternary systems Cu-As-S, Cu-As-Se, and Cu-Sb-S. The results of the studies are published in [12-14, 19, 23, 24, 28, 32, 36, 41, 45, 47, 49, 50-52].

Despite numerous studies devoted to the study of Cu-As(Sb)-X (X = S, Se) systems across various poly- and isothermal sections,

complete phase equilibria have not been obtained before this study. Data on the most studied sections, Cu_2X–$As_2X_3(Sb_2X_3)$, are contradictory, and schematic projections of liquidus surfaces have serious shortcomings: due to insufficient experimental data on the primary crystallization field, most phases are delineated arbitrarily, isotherms are not presented, the precise coordinates of invariant equilibria points are not determined, etc.

When studying phase equilibria in Cu-As-S(Se) systems, particularly for compositions rich in arsenic sulfides (or selenides), numerous published data on the tendency of alloys to form glass were taken into account. Therefore, samples prepared by fusing the starting binary and some ternary compounds with elemental sulfur, as well as glassy alloys of stoichiometric compositions As_2S_3 and As_2Se_3, were subjected to thermal annealing below the solidus for 2000-3000 hours.

It was found that it is precisely after such a long annealing that complete crystallization of the glassy alloys can be achieved, yielding equilibrium samples.

The Cu-As-S System. In Subsection 3.1 of the dissertation, a complete picture of phase equilibria in the Cu-As-S system was obtained through experimental study of alloys thoroughly crystallized by prolonged thermal annealing using differential thermal analysis and powder X-ray diffraction, as well as using available literature data. The liquidus surface projection, the isothermal section at 300 K, and several vertical sections of the phase diagram are presented and discussed. The primary crystallization regions of the phases, as well as the types and coordinates of invariant and univariant phase equilibria, are determined.

Quasi-binary sections and congruent triangulation of the Cu-As-S system. According to our data, the following five sections of the phase diagram are quasi-binary: Cu_2S-As, Cu_2S-Cu_3As, Cu_2S-Cu_3AsS_4, Cu_3AsS_4-S, and Cu_3AsS_4-As_2S_3, which are described in detail in subsection 3.1.1 of this dissertation. Based on the obtained data on quasi-binary sections, a congruent triangulation diagram of the Cu-As-S system was constructed. It was established that, despite the congruent melting nature of AsS, this compound does not

participate in the congruent triangulation of the system.

Solid-phase equilibria in the Cu-As-S system. A combined analysis of experimental data on annealed alloys, taking into account the phase diagrams of boundary binary systems, allowed us to obtain a general picture of solid-phase equilibria in the Cu-As-S system (Fig. 1).

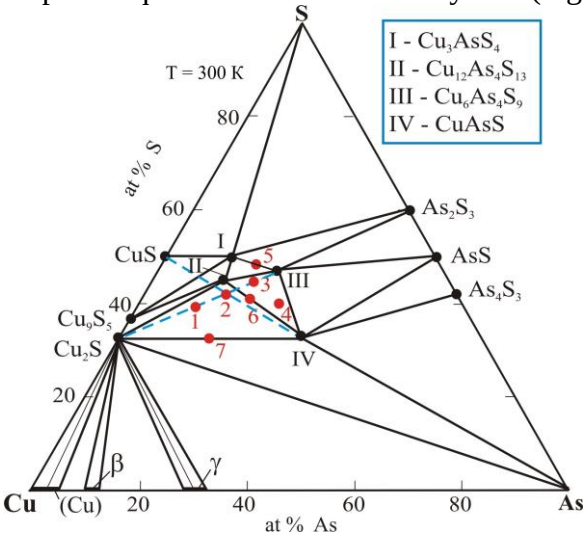

Fig. 1. Solid-phase equilibria diagram of the Cu-As-S system [47]

Table 1.
Crystallographic parameters of ternary compounds of the Cu-As-S system [23, 47]

Compound	**Syngony, Space group and lattice parameters,** Å
α-Cu_3AsS_4	Rombik, *Pmn*2_1, *a* = 7.396, *b* = 6.425, *c* = 6.147
β-Cu_3AsS_4	Tetragonal, *I*-42*m* , *a*=5.287, *c*=10.468
$Cu_{12}As_4S_{13}$	Cubic, *I*-43*m*, *a* = 10.166
$Cu_6As_4S_9$	Triclinic, *a*=9.065, *b*=9.834, *c*=9.072, α=90^0, β=109.5^0, γ=107.7^0
CuAsS	Rombic, *Pnma*, *a* = 11.354, *b* = 3.755, *c* = 5.456

According to the constructed diagram, this system is characterized by the formation of four ternary compounds: Cu_3AsS_4, $Cu_{12}As_4S_{13}$, $Cu_6As_4S_9$, and CuAsS. Fig. 2 shows the powder diffraction patterns

of these compounds. As can be seen, the synthesized samples of these compounds are single-phase and have diffraction patterns similar to those reported in the literature. Crystallographic data obtained from the powder diffraction patterns are presented in Table 1 and also agree well with the literature data.

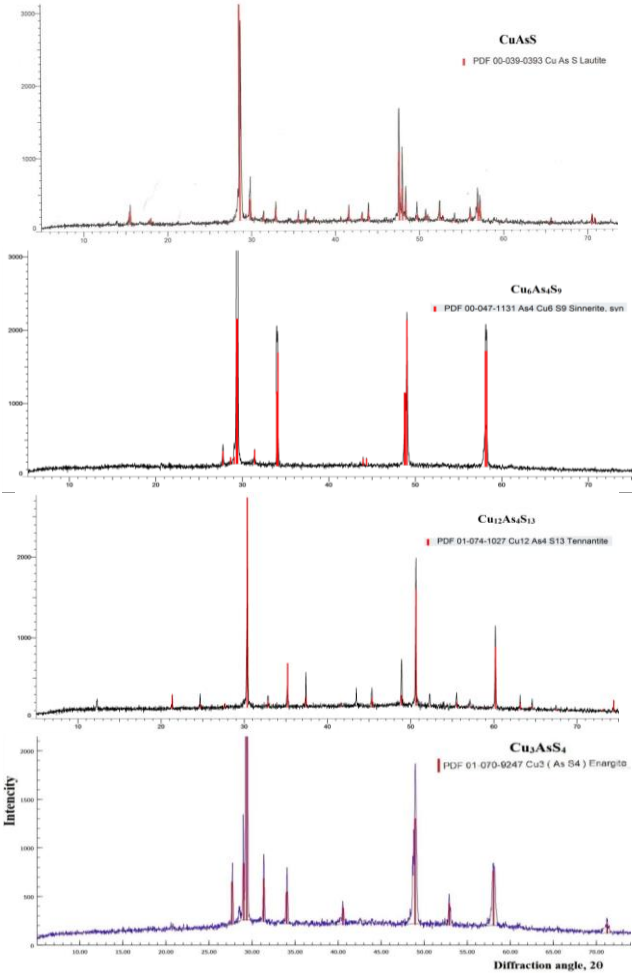

Fig. 2. Powder diffraction patterns of ternary compounds of the Cu-As-S system [47]

a) **b)** **c)**

Fig. 3. SEM images of some alloys of the Cu_2S-As_2S_3 system. (a) - $Cu_{12}As_4S_{13}$; (b) and (c) - samples No. 3 and No. 2 in Fig. 1

We have not confirmed the ternary compounds Cu_5AsS_4, Cu_3AsS_3, and $Cu_4As_2S_5$ reported in the literature (samples 1, 2, and 3 in Fig. 1). Their diffraction patterns consisted of sets of reflection lines from various compounds in this system.

X-ray diffraction analysis also confirmed the presence of other tie lines and three-phase regions. Figure 3 shows SEM images of some alloys. It is easy to verify that they are consistent with Fig. 1.

According to the constructed solid-phase equilibria diagram, the Cu_2S-As_2S_3 section, in contrast to the literature data (Section 1.3), is non-quasi-binary. In the Cu_2S-$Cu_6As_4S_9$ composition range, this section passes through the three-phase regions Cu_2S+$Cu_{12}As_4S_{13}$+ CuAsS and $Cu_{12}As_4S_{13}$+CuAsS+$Cu_6As_4S_9$ (blue dotted line in Fig. 1).

In the Cu-Cu_2S-As composition range, the presence of three three-phase regions delimited by conodes $(Cu_2S)_I$-(Cu), $(Cu_2S)_I$-Cu_8As (β) and $(Cu_2S)_I$-γ was established. The presence of the first two-phase region is due to the formation of up to 6 at% As solid solutions based on Cu in the binary Cu-As system. The $(Cu_2S)_I$ compound also forms concentration tie lines with the $Cu_{12}As_4S_{13}$ and CuAsS compounds, as well as elemental arsenic.

The congruently melting compound Cu_3AsS_4 also plays an important role in the distribution of phase regions, forming tie-rods with six other phases of the system. Three other ternary compounds each form five stable conodes.

Liquidus surface projection. By processing a set of experimental data on quasi-bar and other studied polythermal sections, taking into account literature data on boundary binary systems, a complete and

detailed picture of phase equilibria in the Cu-As-S system was obtained, including a liquidus surface projection (Fig. 4) and several polythermal sections of the T-x-y phase diagram.

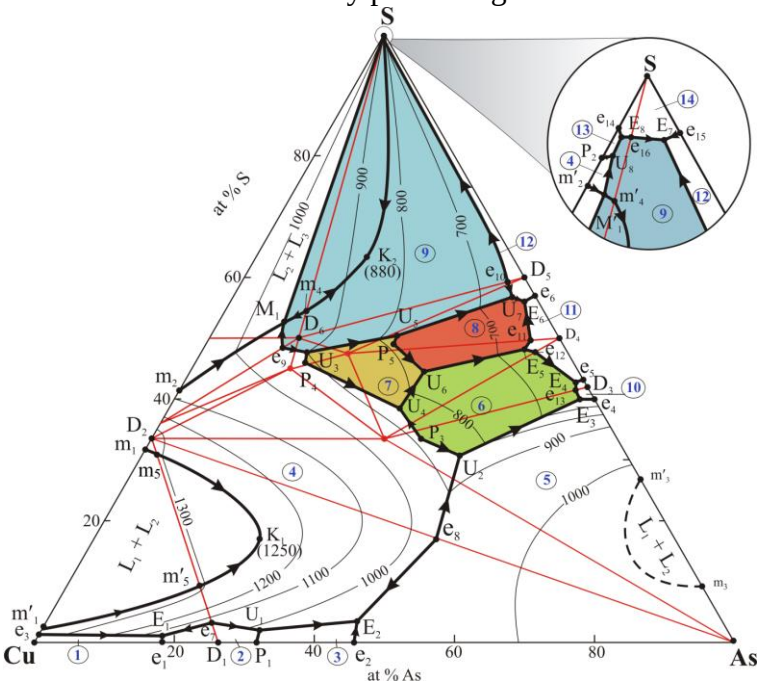

Fig. 4. Projection of the liquidus surface of the Cu-As-S system [47]. Fields of primary crystallization: 1, (Cu); 2, β; 3, γ; 4, (HT-Cu_2S); 5, As; 6, CuAsS; 7, $Cu_{12}As_4S_{13}$; 8, $Cu_6As_4S_9$; 9, Cu_3AsS_4; 10, As_4S_3; 11, AsS; 12, As_2S_3; 13, CuS; 14, S. The red lines show the sections that are stable below the solidus

As can be seen from Fig. 4, the liquidus of this system consists of 14 primary crystallization fields of phases, two of which (CuS and S) are degenerate at the sulfur corner of the concentration triangle. This part of the phase diagram is shown schematically in Figure 4 in an enlarged form. The most extensive crystallization surfaces are those of (HT-Cu_2S), As, and Cu_3AsS_4. The primary crystallization fields of (Cu), as well as the β and γ phases of the binary Cu-As system, extend along this side as narrow bands.

The T-x-y phase diagram of the Cu-As-S system is characterized

by the presence of two wide imiscibility regions L_1+L_2 and L_2+L_3 (L_1 is a Cu-As-based metallic melt; L_2 is a sulfide-based melt; L_3 is a liquid phase rich in elemental sulfur), formed by the penetration (or propagation) of the corresponding regions on the Cu-S boundary system. Fig. 4 shows another stratification region originating from the As-S binary system. However, the boundaries of this region are not precisely established and are marked with dotted lines.

The primary crystallization fields of the phases are delimited by numerous curves of monovariant equilibria and points of nonvariant equilibria. The coordinates of the nonvariant points and the types of the corresponding equilibria are given in Table 2. The types and temperature ranges of monovariant equilibria of the Cu-As-S system are given in the dissertation.

The eutectic curve emanating from point e_8 intersects the L_2+L_3 stratification region and transforms this equilibrium into a four-phase monotectic equilibrium (conjugate points M_1M_1' in Fig. 4).

Table 2

Nonvariant equilibria in the Cu-As-S system [47]

Point in Fig. 4	Equilibrium	**Composition, *at %***		**T, *K***
		As	**S**	
D_1	$L \leftrightarrow \beta$	26.5	-	1100
D_2	$L \leftrightarrow$ (HT- Cu_2S)	-	33.3	1403
D_3	$L \leftrightarrow As_4S_3$	58	42	484
D_4	$L \leftrightarrow AsS$	50	50	591
D_5	$L \leftrightarrow As_2S_3$	40	60	583
D_6	$L \leftrightarrow Cu_3AsS_4$ (I)	12.5	50	970
P_1	$L + \beta \leftrightarrow \gamma$	33	-	982
P_2*	L + (HT- Cu_2S) $\leftrightarrow CuS$	-	>99	780
P_3	L + (HT- Cu_2S) $\leftrightarrow$ CuAsS (IV)	39	33.3	870
P_4	L + (HT- Cu_2S) $\leftrightarrow$ II	16	46	908
P_5	L + II $\leftrightarrow$ III	27	49	795
e_1	$L \leftrightarrow$ (Cu)+ β	18.2	-	958
e_2	$L \leftrightarrow \gamma$ + As	46	-	873
e_3	$L \leftrightarrow$ (Cu) + (HT- Cu_2S)	-	1.5	1340
e_4	$L \leftrightarrow As + As_4S_3$	40	60	475
e_5	$L \leftrightarrow AsS + As_4S_3$	57	43	480
e_6	$L \leftrightarrow AsS + As_2S_3$	43	57	580
e_7	$L \leftrightarrow \beta$ + (HT- Cu_2S)	23.5	3	1070
e_8	$L \leftrightarrow As$ + (HT- Cu_2S)	50	17.5	985

e_9	L ↔ (HT- Cu_2S) + I	11	48	960
e_{10}	L ↔ As_2S_3 + I	38	59.5	580
e_{11}	L ↔ AsS + II	46	49.5	585
e_{12}	L ↔ AsS + IV	48	48	583
e_{13}	L ↔ As_4S_3 + IV	56	42	480
e_{14}^*	L ↔ CuS + S		>99	388
e_{15}^*	L ↔ As_2S_3 + S		>99	388
e_{16}^*	L ↔ Cu_3AsS_4 + S		>99	388
m_1 (m_1')	L_2 ↔ L_1+ (HT- Cu_2S)	-	2 (32.9)	1380
m_2 (m_2')	L_2 ↔ L_3+ (HT- Cu_2S)	-	41 (>99)	1086
m_3 (m_3')	L_1↔ L_2 + As	91 (73)	9 (27)	1050
m_4 (m_4')	L_2 ↔ L_3+ I	11.5	55	960
m_5 (m_5')	L_2 ↔ L_1+ (HT- Cu_2S)	2 (18.5)	31 (9.5)	1310
M_1 (M_1')	L_2 ↔ L_3+ (HT- Cu_2S)+ I	9	53	950
U_1	L+β ↔ (HT- Cu_2S) + γ	33	2	968
U_2	L+(HT- Cu_2S)↔ As + IV	46	31	845
U_3	L+(HT- Cu_2S) ↔ I + II	15	47	900
U_4	L+(HT- Cu_2S) ↔ II + IV	33	38	858
U_5	L+ II ↔ I + III	26	51	790
U_6	L+ II↔III + IV	33	45	770
U_7	L+ I ↔ As_2S_3 + III	40	57	575
U_8^*	L+ (HT- Cu_2S)↔CuS + Cu_3AsS_4	-	>99	770
E_1	L↔(Cu) + β + (HT- Cu_2S)	17.5	1	940
E_2	L ↔ As+ γ +(HT- Cu_2S)	44.5	3	855
E_3	L ↔ As + AsS +IV	59	40	470
E_4	L ↔ As_4S_3 + AsS +IV	56	43	475
E_5	L ↔ AsS + III + IV	46	48	580
E_6	L ↔ AsS + As_2S_3 + III	42	56	570
E_7^*	L ↔ CuS + I + S		>99	~388
E_8^*	L ↔ I + As_2S_3 + S		>99	~388

**Points degenerated near the sulfur angle are marked with an asterisk.*

** I- Cu_3AsS_4; II - $Cu_{12}As_4S_{13}$; III - $Cu_6As_4S_9$; IV - CuAsS.

Polythermal section Cu_2S-As_2S_3. According to our data, in contrast to previously proposed variants of the phase diagram, this section is not quasi-binary. As shown above, below the solidus in the composition range of 0-40 mol% As_2S_3, it passes through the three-phase fields Cu_2S+II+IV and II+III+IV. This is because compound II, which is not located in this section by composition, forms a tie-line with CuAsS (IV). Compound $Cu_6As_4S_9$ located in this section forms a tie-line with As_2S_3, i.e., in the composition range ≥60 mol%

As_2S_3, the section is stable (III+As_2S_3). Crystallization is complex. In Fig. 5, from left to right, (HT-Cu_2S), II, I, and As_2S_3primarily crystallize from the melt. Comparison of Fig. 5 with 4 shows that the curves located below the liquidus (P_4U_4, U_4U_6, $U_6P_5U_5$) reflect the monovariant equilibria L+(HT-Cu_2S)↔II, L↔II+IV and L+II↔IIII, respectively.

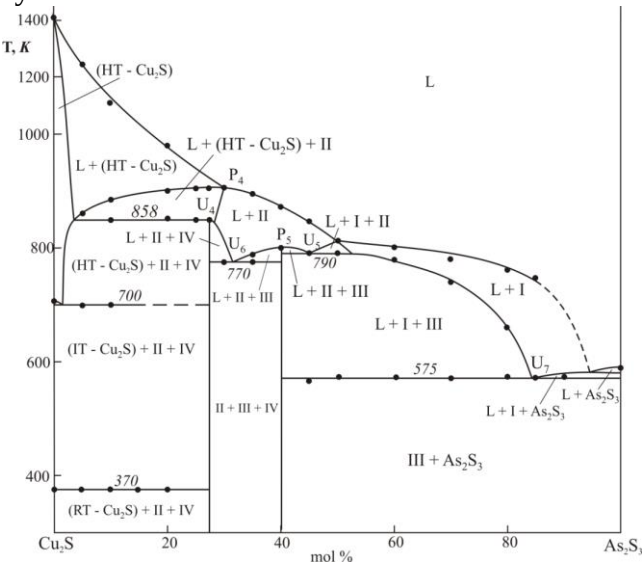

Fig. 5. Polythermal section of Cu_2S-As_2S_3 [47]

The dissertation also constructs the following polythermal sections of the T-x-y diagram, which more clearly demonstrate the crystallization processes and solid-phase transformations in the system: CuS-AsS, Cu_2S-"As_2S", CuS-As, Cu-AsS, [$Cu_{0,8}S_{0,2}$]-As, 4CuS-Cu_3AsS_4, Cu_2S-[A], Cu_3AsS_4-[B], [A]-As_2S_3.

The Cu-As-Se system. Section 3.2 of the dissertation presents data on quasi-binary sections, congruent triangulation, and solid-phase equilibria in this system, as well as a projection of the liquidus surface.

According to the obtained experimental data, the following sections of the phase diagram of the Cu-As-Se system are quasi-binary or partially quasi-binary: Cu-As-Se: Cu_2Se-As, Cu_2Se-Cu_3As, Cu_2Se-As_2Se_3, Cu_2Se-Cu_3AsSe_4, Cu_3AsSe_4-Se, and Cu_3AsSe_4-

As_2Se_3.

The presented data on quasi-binary sections allow for a congruent triangulation of the Cu-As-Se system. This system can be represented as a set of six subordinate subsystems: Cu-Cu_2Se-Cu_3As, Cu_2Se-Cu_3As-Se, Cu_2Se- Cu_3AsSe_4-Se, Cu_3AsSe_4-As_2Se_3-Se, Cu_2Se-Cu_3As-As_2Se_3, and Cu_2Se-As_2Se_3-As.

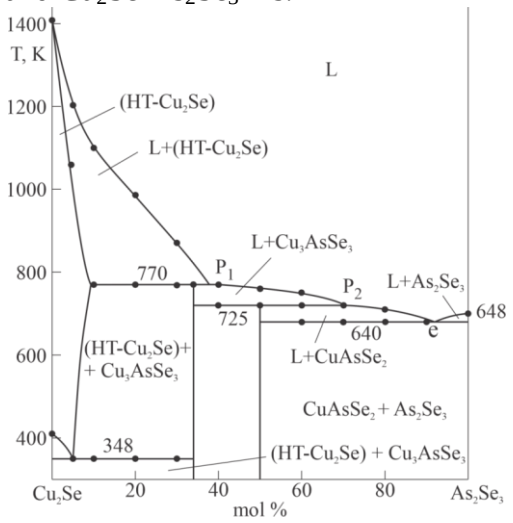

Fig. 6. Quasi-binary section Cu_2Se-As_2Se_3 [50, 52]

The Cu_2Se-As_2Se_3 section was re-investigated, and its refined phase diagram was constructed (Fig. 6). It was shown that this system is quasi-binary and is characterized by the formation of ternary compounds Cu_3AsSe_3 and $CuAsSe_2$, which melt with decomposition via peritectic reactions at 770 and 725 K, respectively.

Solid-phase equilibria in the Cu-As-Se System.

A generalization of experimental results on annealed alloys, combined with phase diagrams of the corresponding boundary binary systems, made it possible to establish a general picture of solid-phase equilibria in the Cu-As-Se system (Fig. 7).

According to the constructed solid-phase equilibria diagram (Fig. 7), this system is characterized by the formation of five ternary compounds: Cu_3AsSe_4, Cu_3AsSe_3, $Cu_7As_6Se_{13}$, $CuAsSe_2$, and

CuAsSe. The obtained powder diffraction patterns and crystallographic data for these compounds are in good agreement with the literature. The ternary compounds $Cu_4As_2Se_5$ and $Cu_6As_4Se_9$, mentioned in the literature, have not been confirmed by us. Their X-ray diffraction patterns consisted of sets of reflection lines from various compounds in this system.

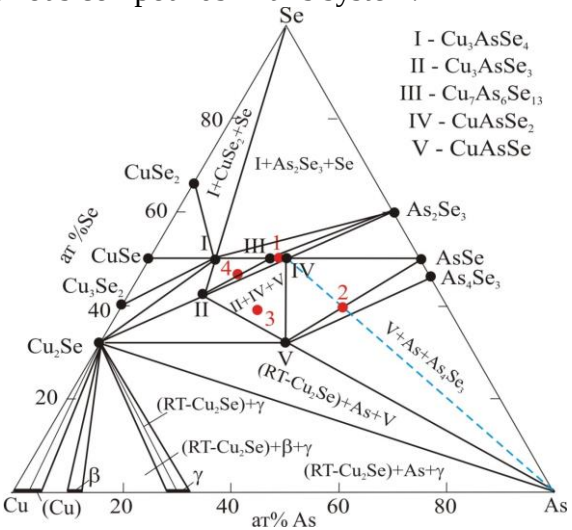

Fig. 7. Solid-phase equilibria diagram of the Cu-As-Se system at 300 K [52]

Liquidus surface projection. The liquidus of the Cu-As-Se system consists of 15 primary crystallization fields of the phases (Fig. 8). Three of these fields correspond to the initial components, seven to the binary compounds formed at the boundary systems, and five regions to the copper-arsenic selenides. The primary crystalization fields of HT-CuSe (P_3), $CuSe_2$ (P4), and $Cu_7As_6Se_{13}$ (P_7) compounds are degenerate and are shown in Fig. 8 in an enlarged form (scale is arbitrary).

The most extended crystallization surfaces are HT-Cu_2Se), As, Cu_3AsSe_4, and Cu_3AsSe_3. The T-x-y phase diagram of the Cu-As-Se system is characterized by the presence of two wide stratification regions L_1+L_2 and L_2+L_3 (L_1 is a Cu-As-based metallic melt; L_2 is a

selenide-based melt; L_3 is a liquid phase rich in elemental selenium), formed by the penetration of the corresponding regions on the Cu-Se boundary system.

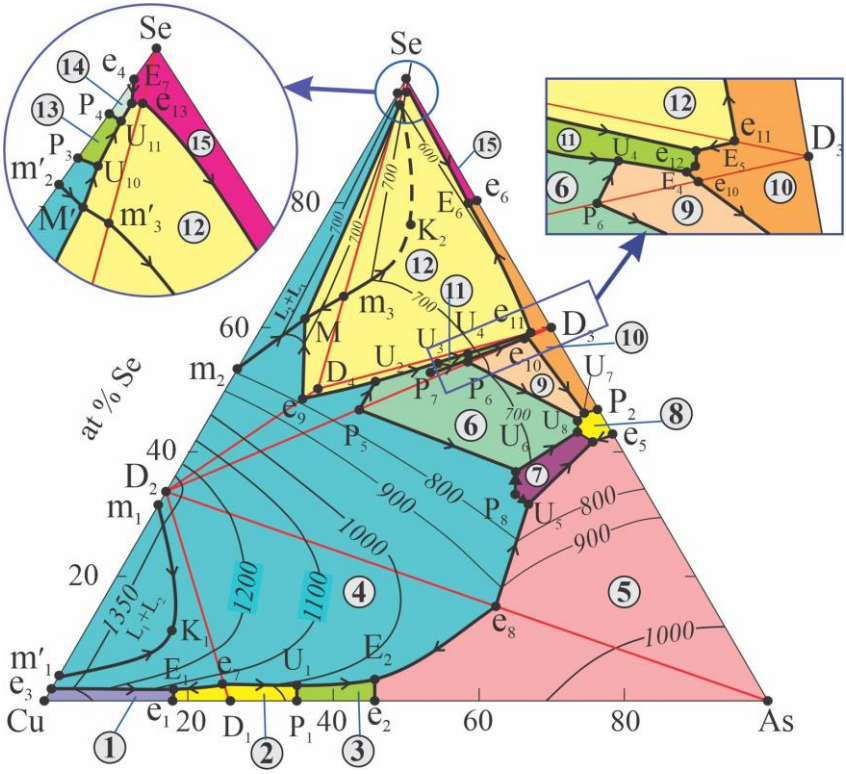

Fig. 8. Projection of the liquidus surface of the Cu-As-Se system [52]. Fields of primary crystallization of phases: **1** - (Cu); **2** - γ; **3** - δ; **4** - (HT-Cu_2Se); **5** – As; **6** - Cu_3AsSe_3; **7** – CuAsSe; **8** – AsSe; **9** - $CuAsSe_2$; **10** – As_2Se_3; **11** - $Cu_7As_6Se_{13}$; **12** - Cu_3AsSe_4; **13** - (HT-CuSe); **14** - $CuSe_2$; **15** – Se

The primary crystallization fields of the phases are delimited by numerous curves of monovariant equilibria and points of nonvariant equilibria. The coordinates and types of nonvariant and monovariant equilibria of the system are given in the dissertation.

The eutectic curve emanating from point e_9 intersects the immiscibility region L_2+L_3 and transforms this equilibrium into a

four-phase monotectic equilibrium (conjugate points M_1M_1' in Fig. 8).

In conclusion of this section, we note that the experimentally obtained liquidus surface projection for this system exhibits a significantly more complex picture of phase equilibria compared to that presented in the literature, which only reflects two ternary compounds, Cu_3AsSe_4 and $CuAsSe_2$.

Furthermore, the dissertation examines in detail 11 polythermal sections of the Cu-As-Se system.

The Cu-Sb-S system. Section 3.3 of the dissertation presents a complete picture of phase equilibria in the Cu-Sb-S system. The liquidus surface projection, the isothermal section at 300 K, and several vertical sections of the phase diagram are presented and discussed. The primary crystallization fields of the phases, as well as the types and coordinates of non- and monovariant phase equilibria, are determined.

Further in the text, in the figures, and in the tables, the following designations of phases are adopted: I - Cu_3SbS; II - $CuSbS_2$; III- $Cu_{12}Sb_4S_{13}$; IV - $Cu_{14}Sb_4S_{13}$; V - Cu_3SbS_3. Phases based on high-temperature, intermediate, and low-temperature modifications of Cu2S are designated, respectively, (HT- Cu_2S), (IT-Cu_2S), (RT-Cu_2S). Intermetallic phases of the Cu-Sb system are designated by Greek letters, γ, δ, η.

The solid-phase equilibria diagram of the Cu-Sb-S system at 300 K is constructed based on the X-ray diffraction data for the alloys of the system. This diagram differs slightly from the phase diagram at 570 K given in the literature. The main difference is that Fig. 9, in addition to the ternary compounds $CuSbS_2$, Cu_3SbS_4, and $Cu_{12}Sb_4S_{13}$, also contains Cu_3SbS_3 and $Cu_{14}Sb_4S_{13}$ as separate phases. The $Cu_{14}Sb_4S_{13}$ compound is a variety of tetrahedrite mineral with the highest copper content (Table I), and its composition lies on the Cu_2S-Sb_2S_3 section (22.22 mol.% Sb_2S_3). It was found that this compound forms conode lines with elemental antimony and with the $Cu_{12}Sb_4S_{13}$ compound. The presence of a conod between the $Cu_{14}Sb_4S_{13}$ and $Cu_{12}Sb_4S_{13}$ phases is clearly visible in Fig. 9.

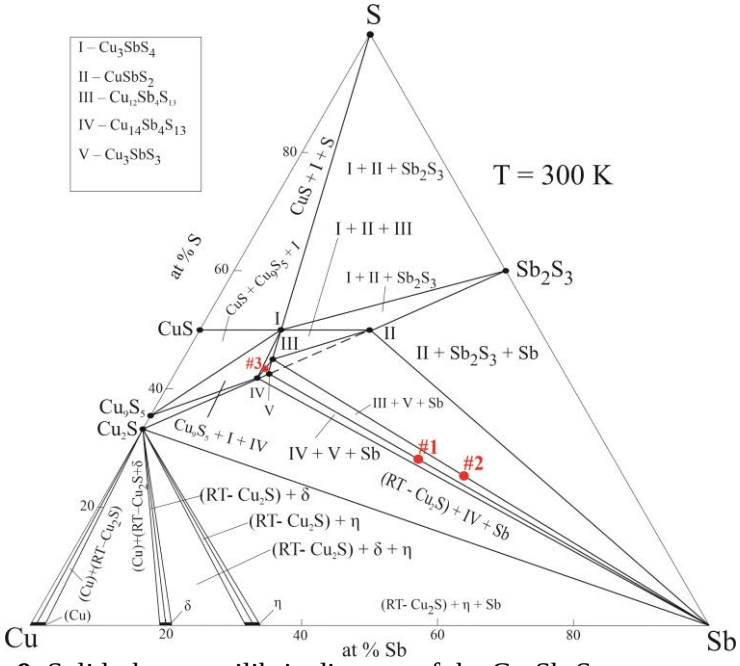

Fig. 9. Solid-phase equilibria diagram of the Cu-Sb-S system at room temperature [41]

The cubic lattice parameters of these phases, determined from the diffraction pattern, are: a = 10.3084 (7) Å and a = 10.4473 (7) Å, which are practically identical to the literature data for the stoichiometric compositions $Cu_{12}Sb_4S_{13}$ and $Cu_{14}Sb_4S_{13}$, respectively. It should be noted that the existence of a cubic phase in the Cu_2S-Sb_2S_3 section has previously been noted in the literature. However, the authors considered this phase to be a low-temperature modification of Cu_3SbS_3 with a slight compositional shift toward Cu_2S.

The obtained X-ray diffraction patterns confirm the conode lines of Cu_3SbS_4 - $Cu_{12}Sb_4S_{13}$ and $CuSbS_2$ - $Cu_{12}Sb_4S_{13}$. However, contrary to the literature, it was found that the Cu_3SbS_3 and $CuSbS_2$ compounds do not exhibit a conode lie. Alloys in this composition range contain elemental antimony.

The powder diffraction patterns presented in the dissertation

clearly demonstrate the presence of $Cu_{12}Sb_4S_{13}$-Sb (alloy #2 in Fig. 9) and Cu_3SbS_3-Sb (alloy #1 in Fig. 9) conodes. This means that the Cu_3SbS_3-$CuSbS_2$ tie-line does not exist. In addition, the alloy of the composition "$C_{13}Sb_4S_{13}$" (alloy #3 in Fig. 9) consists of a two-phase mixture of $Cu_{12}Sb_4S_{13}$ and $Cu_{14}Sb_4S_{13}$ tetrahedrites. This shows that, despite the isostructural nature and closeness of the lattice parameters of these two limiting tetrahedrite compositions, their mutual solubility is low. This is probably due to the structural features of $Cu_{12}Sb_4S_{13}$ and $Cu_{14}Sb_4S_{13}$.

Liquidus surface. As can be seen from Fig. 10, the liquidus surface of this system consists of 13 primary crystallization fields of the phases. The crystallization fields of CuS and S are degenerate at the sulfur corner of the concentration triangle. This part of the phase diagram is shown schematically in an enlarged form (Fig. 10a). The primary crystallization fields of (Cu) and the β and η phases of the binary Cu-Sb system extend along this side as narrow bands.

A characteristic feature of the Cu-Sb-S system is that it has two wide stratification regions L_1+L_2 and L_2+L_3 (L_1 is a Cu-Sb-based metallic melt; L_2 is a sulfide-based melt; L_3 is a sulfur-based liquid phase). These regions (shaded areas in Fig. 10) appear as wide, continuous bands between the stratification regions of the Cu-S and Sb-S boundary binary systems and occupy ~90% of the total area of the concentration triangle.

The primary crystallization fields of the phases are delimited by numerous curves of monovariant equilibria and points of nonvariant equilibria. The coordinates of the nonvariant points and the types of corresponding equilibria, as well as the types and temperature ranges of monovariant equilibria, are given in the dissertation.

Some curves of monovariant equilibria intersect the stratification regions and, in doing so, are transformed into four-phase monotectic equilibria (conjugate points M_1–M_1', M_2–M_2', and M_3–M_3' in Fig. 10).

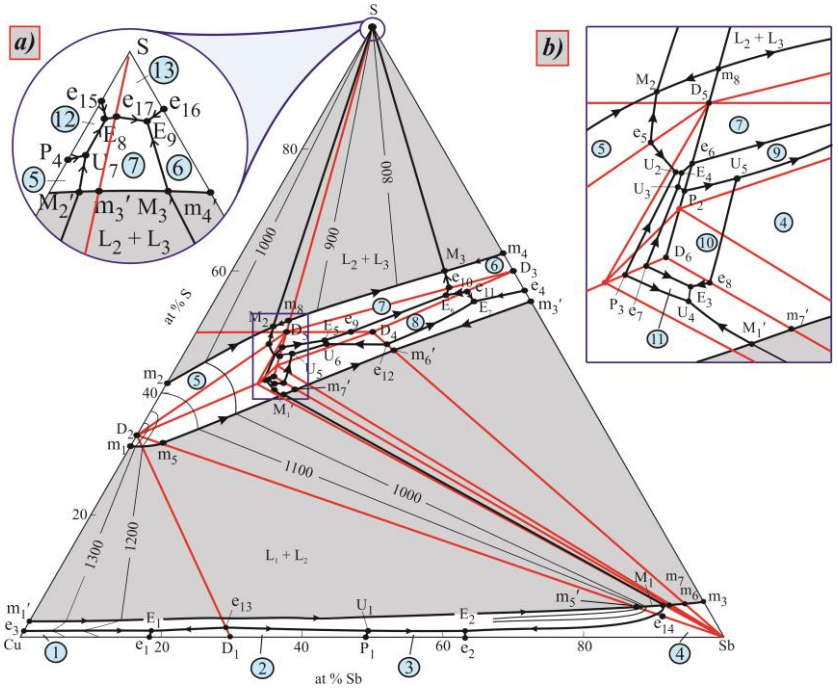

Fig. 10. Projection of the liquidus surface of the Cu-Sb-S system [45]. Fields of primary crystallization of phases: **1**- (Cu); **2**- β-фаза; **3** - η-фаза; **4** – Sb; **5** – (HT-Cu_2S); **6** – Sb_2S_3; **7** –Cu_3SbS_4; **8** – $CuSbS_2$; **9** – $Cu_{12}Sb_3S_{13}$; **10** – Cu_3SbS_3; **11** - $Cu_{14}Sb_3S_{13}$; **12** – CuS; **13** –S. Red lines show sections that are stable below the solidus.

The complex nature of phase equilibria in a narrow compositional region, highlighted by a rectangle and shown in an enlarged view (Fig. 10b), should be noted.

Polythermal section of Cu_2S-Sb_2S_3. To clarify the interfaces between the primary crystallization fields of the phases and the coordinates of the invariant equilibria points on the T-x-y phase diagram of the Cu-Sb-S system, a series of polythermal sections was constructed. Only the Cu_2S-Sb_2S_3 section (Fig. 11), which we have studied in detail and for which there is considerable conflicting data in the literature, is presented here.

In the composition range ≥50 mol% Sb_2S_3, the obtained results coincide with the data of the above-mentioned studies, according to

which this part of the system is quasi-binary and belongs to the eutectic type. According to our data, the region ≤25 mol% Sb_2S_3 is also quasi-binary. This part of the phase diagram is characterized by the formation of the $Cu_{14}Sb_4S_{13}$ compound, a synthetic analogue of tetrahedrite with the maximum copper content, by the peritectic reaction L+(HT-Cu_2S)↔$Cu_{14}Sb_4S_{13}$ at 870 K. The peritectic point has a composition of ~23 mol% Sb_2S_3. The compound $Cu_{14}Sb_4S_{13}$ forms a eutectic (e7) with congruently melting Cu_3SbS_3, which has a composition of ~24 mol% Sb_2S_3 and crystallizes at 863 K. The horizontal at 695 K corresponds to the eutectoid equilibrium (HT-Cu_2S)↔(IT-Cu_2S)+$Cu_{14}Sb_4S_{13}$.

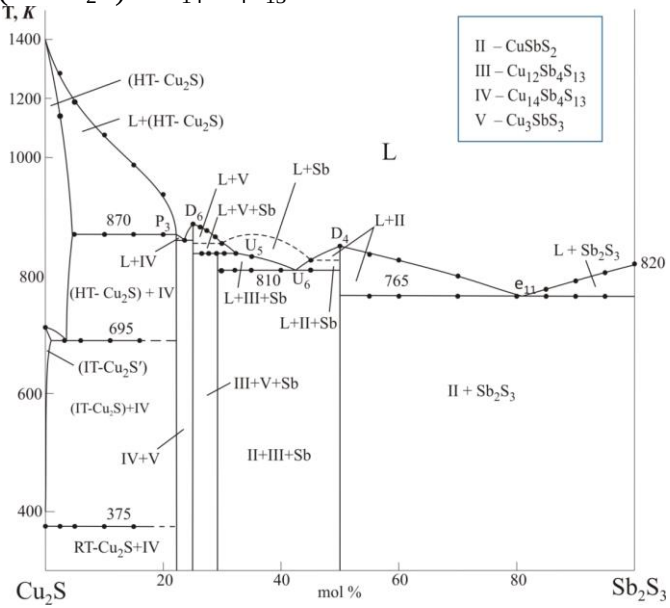

Fig. 11. Phase diagram of the Cu_2S-Sb_2S_3 system [41]

In the intermediate composition range (25-50 mol% % Sb_2S_3), the Cu_2S-Sb_2S_3 section is not quasi-binary. The powder X-ray diffraction patterns presented in the dissertation convincingly demonstrate the presence of a tie bond between the tetrahedrite phase – $Cu_{12}Sb_4S_{13}$, which is compositionally outside this section, and elemental antimony. This leads to the formation of three-phase regions Cu_3SbS_3+$Cu_{12}Sb_4S_{13}$+Sb and $Cu_{12}Sb_4S_{13}$+$CuSbS_2$+Sb in the

composition range of 25-50 mol% (Fig. 11).

Comparison of Fig. 10 with Fig. 11 shows that in the composition ranges of 25-30, 30-45, and 45-50 mol% Sb_2S_3, Cu_3SbS_3, Sb, and $CuSbS_2$, respectively, primarily crystallize from the melt. The liquidus of elemental antimony is not experimentally recorded due to the insignificant amount of the crystallizing phase and the large steepness of the liquidus surface (Fig. 10); it is represented by the dotted curve (Fig. 11). The intersection points of this curve with the liquidus curves of two adjacent phases (the intersection of this section with the eutectic curves e_8U_5 and $e_{12}U_6$ in Fig. 11) correspond to the onset of the monovariant eutectic processes $L \leftrightarrow Cu_3SbS_3+Cu_{12}Sb_4S_{13}$ and $L \leftrightarrow Cu_{12}Sb_4S_{13}+CuSbS_2$. These processes lead to the formation of three-phase fields L+V+Sb and L+II+Sb, respectively, on the phase diagram (Fig. 11). The horizontal line at 835 K (U_5) corresponds to the invariant transition reaction $L+V \leftrightarrow Sb+III$. In a narrow composition range of ~25–28 mol% Sb_2S_3, crystallization is completed by this reaction, and a three-phase mixture III+V+Sb is formed. In the composition range >28 mol% Sb_2S_3, crystallization continues according to the monovariant eutectic reaction U_5U_6 and is completed by the invariant transition reaction (U_6) at 810 K. As a result, a three-phase region II+III+Sb is formed in the subsolidus.

Some features of phase formation and phase equilibria in A^I-B^V-X (A^I – Cu, Ag; B^V – As, Sb; X – S, Se)

By summarizing the results obtained for six systems (Cu-As-S, Cu-As-Se, Cu-Sb-S, Ag-As-S, Ag-As-Se, Ag-Sb-Se) and literature data for the remaining two systems (Cu-Sb-Se, Ag-Sb-S) of this type, the dissertation highlights some features of phase formation and phase equilibria in them (Section 3.4).

Phase formation. First of all, it should be noted that the specified systems are rich in ternary compounds (29 compounds in total), and most of them are found in nature in the form of minerals: enargite ($(\alpha$-$Cu_3AsS_4)$, luisonite (β-Cu_3AsS_4), synnerite ($Cu_6As_4S_9$), tennantite ($Cu_{12}As_4S_{13}$), chalcostibite ($CuSbS_2(Se_2)$, skinnerite ($Cu_3SbS_3(Se_3)$, famatinite ($Cu_3SbS_4(Se_4)$), tetrahedrite $Cu_{12+x}Sb_{4+y}S_{13}(Se_{13})$, $0 \le x \le 1.92$

and $0.02 \leq y \leq 0.27$), trehmannite and smithite ($AgAsS_2$), xanthoconite and proustite $Ag_3AsS_3(Se_3)$, dervillite (Ag_2AsS_2), pierceite ($Ag_{16}As_2S_{11}$), etc.

An analysis of the phase diagrams shows that ternary compounds are formed primarily in the A^I_2X-$B^V_2X_3$ sections. In these compounds, the copper and silver atoms have an oxidation state of 1+, while the arsenic and antimony atoms have an oxidation state of 3+. The most characteristic compounds are $A^IB^VX_2$, which exist in seven of the ternary systems considered. In the Cu-As-S system, instead of $CuAsS_2$, there is a compound with a similar composition, $Cu_6As_4S_9$ (the mineral synnerite). Another characteristic type of compound is $A^I_3B^VX_3$, which is found in six of the eight systems. In the Cu-As-S and Cu-Sb-S systems, there are compounds with similar compositions, $Cu_{12}As_4S_{13}$ and $Cu_{12}Sb_4S_{13}$. Both of these compounds deviate slightly in composition from the above sections towards an excess of sulfur. This leads to an increase in the oxidation state of some copper atoms to 2+.

In all systems except Ag-Sb-Se, ternary compounds exist outside the A^I_2X-$B^V_2X_3$ sections. In copper-based systems, these are $Cu_3B^VX_4$ and CuAsX, while in silver-based systems, these are $Ag_7B^VX_6$ compounds. In the $Cu_3B^VX_4$ compounds, copper apparently exists as Cu^+ ions, while arsenic and antimony have the 5+ oxidation state. Similar oxidation states are also exhibited by Ag and B^V atoms in $Ag_7B^VX_6$ compounds. It should be noted that the 5+ oxidation state is not realized in binary B^V-X systems, with the exception of As_2S_5, which exists at high pressures. Thus, the presence of Ag and Cu atoms in the system leads to the realization of the maximum oxidation state of arsenic and antimony in their chalcogenide compounds.

As for CuAsX compounds, the chalcogen atoms are most likely bonded to copper through an arsenic atom.

Phase equilibria. Analysis of the phase diagrams of the A^I-B^V-X systems, their vertical and isothermal sections, shows that in six of the eight systems, the A^I_2X-$B^V_2X_3$ type sections are quasi-binary, and in seven, the A^I_2X-B^V sections are also quasi-binary. In type 1 systems, various intermediate compounds are formed, while in type 2

systems, chemical interaction is absent. The phase diagrams of the latter belong to the type with monotectic and eutectic equilibria. It should be especially noted that among the A^I_2X-$B^V_2X_3$ type sections (Fig. 12), Cu_2S-As_2S_3 and Cu_2S-Sb_2S_3 are non-quasi-binary, in which synthetic analogues of the minerals tennantite and tetrahedrite ($Cu_{12}As_4S_{13}$ and $Cu_{12}Sb_4S_{13}$) exist. These compounds form stable junctions with elemental pnictogen, which disrupts the stability of these sections.

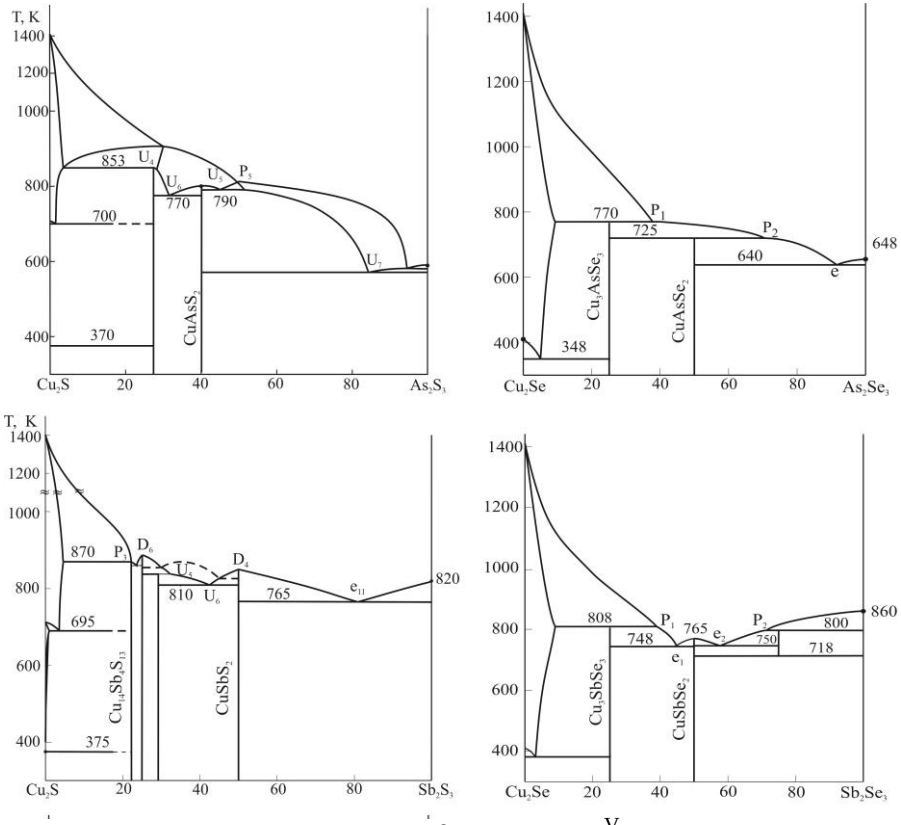

Fig. 3.4.1. Phase diagrams of the Cu_2X-$B^V_2X_3$ systems [49]

Solid-phase equilibria diagrams (Fig. 13) clearly demonstrate the degree of influence of ternary compounds on the distribution of phase regions. In particular, the quasi-binary nature of the A^I_2X-B^V sections significantly limits the range of compositions in which

ternary compounds participate in the formation of heterogeneous phase fields. In all systems, with the exception of Ag-Sb-S, ternary compounds do not participate in phase equilibria in the A^{I}-$A^{I}_{2}X$-B^{V} composition range. It should be noted that in most of the systems under consideration, ternary compounds most saturated with chalcogen form stable tie bonds with it, while those rich in arsenic and antimony form stable tie bonds with the latter.

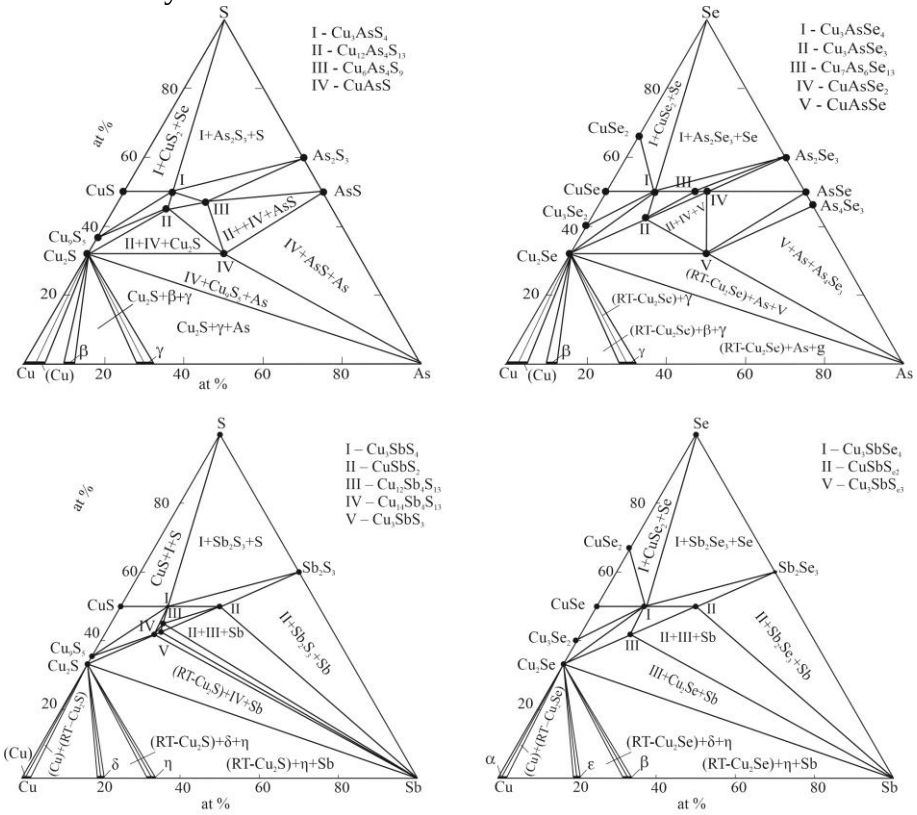

Fig. 13. Solid-phase equilibria diagrams of Cu-B^{V}-X systems at 300 K [49]

A comparison of the liquidus surface projections (Fig. 14) for the systems examined shows that the largest areas are occupied by the primary crystallization fields of $A^{I}_{2}X$ compounds and elemental arsenic and antimony, while among the ternary phases, congruently

melting compounds of the $Cu_3B^VX_4$ and AgB^VX_2 types occupy the largest areas. All of these ternary systems are characterized by the presence of two or three stratification regions in the liquid state. These stratification regions originate from the boundary binary systems A^I-X and B^V-X. In the two sulfide systems Cu-Sb-S and Ag-Sb-S, the stratification regions emanating from these boundary systems merge to form two continuous stratification bands, which cover over 90% of the area of the corresponding concentration triangle.

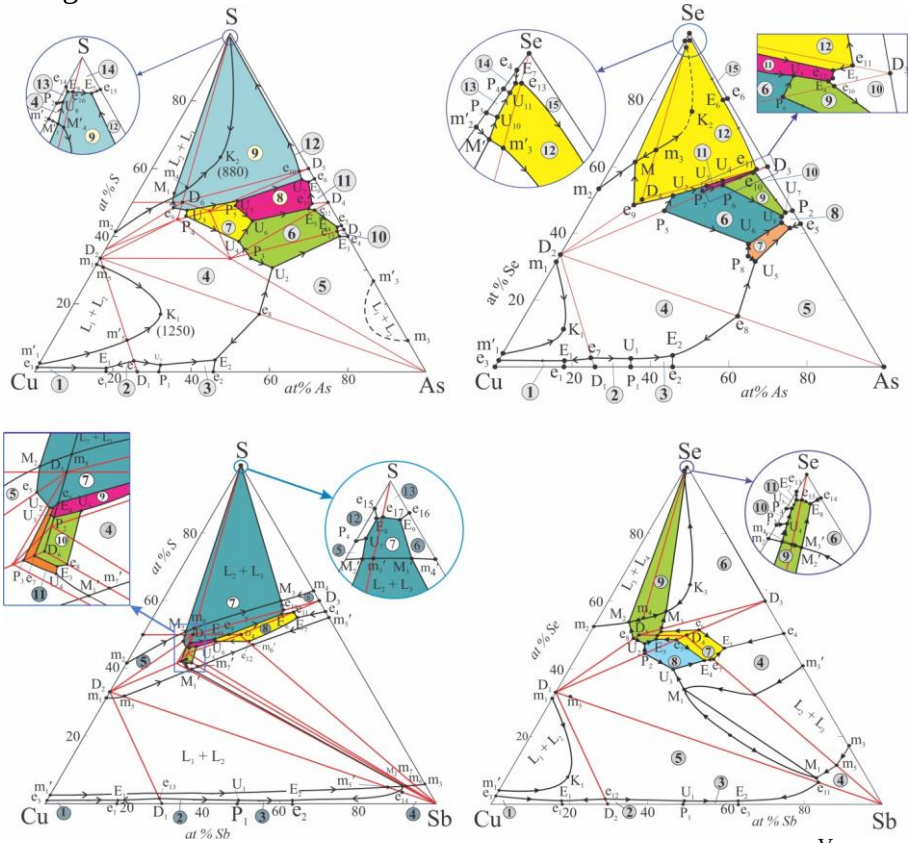

Fig. 14. Projections of the liquidus surfaces of some Cu-B^V-X systems [49]. *Colored fields are areas of primary crystallization of ternary compounds*

In the fourth chapter, phase equilibria in some quasi-ternary systems of the Ag_2X-$A^{IV}X$-$B^V{}_2X_3$ (A^{IV}- Ge, Sn, Pb; B^V-Sb, Bi; X – Se, Te) and quaternary Cu-Ge-Sb-X (X is S, Se) systems along the Cu_3SbX_4-GeX_2 sections are investigated. It is known that tellurides of heavy p-metals and their derivative phases are very attractive for high technologies due to their unique physical properties. Binary compounds $A^{IV}Te$ and $B^V{}_2Te_3$, as well as homologous series of ternary phases $n(A^{IV}Te)\cdot m(B^V{}_2Te_3)$ exhibit promising thermoelectric properties. The research results are presented in [3, 7, 11, 16, 17, 20-22, 29-31, 33, 35, 38, 40, 43, 44].

Ag_2Te-$SnTe$-Sb_2Te_3 system. Section 4.1 presents the results of the study of phase equilibria in the Ag_2Te-$SnTe$-Sb_2Te_3 system.

Solid-phase equilibria. Isothermal sections at 700 K and 400 K of the phase diagram of the Ag_2Te-$SnTe$-Sb_2Te_3 system were constructed. In the Ag_2Te-$SnTe$-Sb_2Te_3 system, a wide (up to 9 mol.%) continuous band of a solid solution (β-phase) is formed at 700 K, covering the SnTe-«$AgSbTe_2$» section (composition range >15 mol.% SnTe) and the SnTe-ε-phase section (Fig. 15). In addition, solid solutions based on the intermediate modification of Ag_2Te (α-phase), Sb_2Te_3 (γ-phase), and $SnSb_2Te_4$ (δ-phase) are also observed in this system at 700 K. The α-phase has a homogeneity region of >95 mol.% Ag_2Te, and the γ- and δ-phases are located in narrow bands (1-2 mol.% wide), covering composition ranges of 43-56 and 87-100 mol.% Sb_2Te_3, respectively.

These phases with variable composition form between themselves wide two-phase α+β, β+γ, and β+δ regions. Between the last two regions, a three-phase β+γ+δ region is formed (Fig. 15).

The isothermal section at 400 K has a slightly different phase equilibria pattern (Fig. 15). This is due to two factors. First, at 600–630 K, the ε-phase and β-phase with a content of <15 mol.% SnTe decomposes according to the eutectoid reaction ε(β)↔α+γ, and the homogeneity region of the β-phase narrows. Second, at 415 K, the invariant eutectoid equilibrium α↔RT-Ag_2Te+β+γ is established. As a result, the RT-Ag_2Te+β+γ phase region is formed in the system, and the β+γ region narrows somewhat. It should be noted that Fig. 15 also reflects phase equilibria at room temperature, since phase

transitions below 415 K are not observed.

The location and boundaries of the phase regions on the solid-phase equilibrium diagrams (Fig. 15) were established using the XRD method and confirmed by the DTA method, as well as by microhardness and EMF measurements.

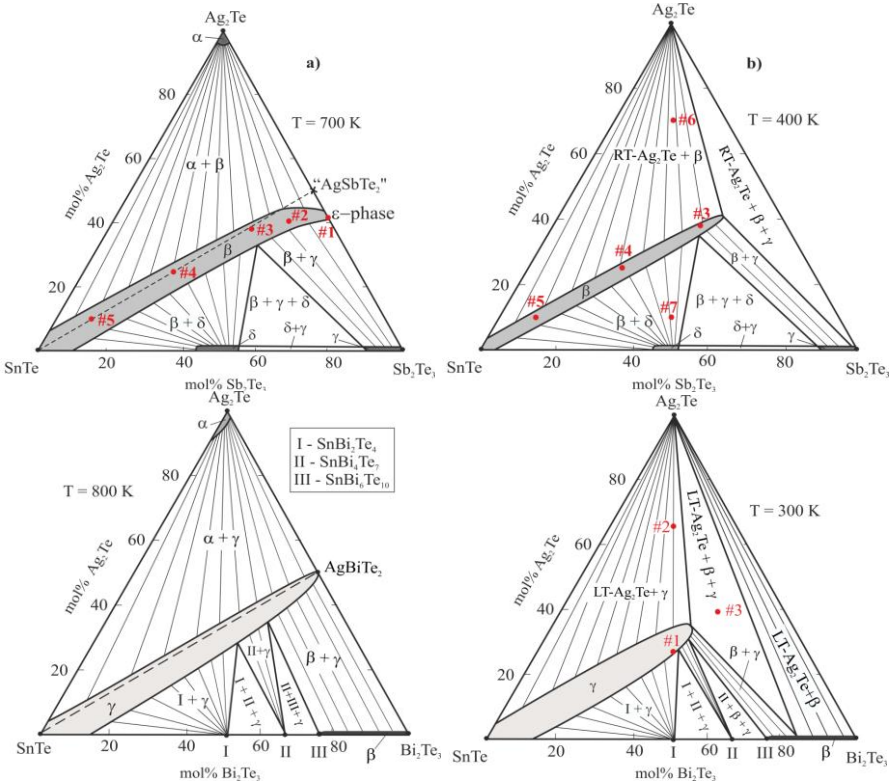

Fig. 15. Isothermal sections of phase diagrams of the Ag_2Te-SnTe-Sb_2Te_3 [22] and Ag_2Te-SnTe-Bi2Te3 [21] systems

Figure 16 shows the powder X-ray diffraction patterns of selected alloys 1–7 from Fig. 15. Alloys 1 and 2 were quenched from 700 K after annealing, while the remaining alloys (3–7) were further annealed at 400 K after a long heat treatment at 700 K. The X-ray diffraction patterns of alloys 1–5 have qualitatively the same diffraction pattern characteristic of a cubic structure, and some shift

of the reflection peaks is observed with a change in the alloy composition (Fig. 16a). The X-ray diffraction patterns of two other selected samples, #6 and #7 (Fig. 16b), confirm their two-phase composition and consist of a set of reflection lines of RT-Ag_2Te and the β-phase (for alloy #6) and the β- and δ-phase (for alloy #7).

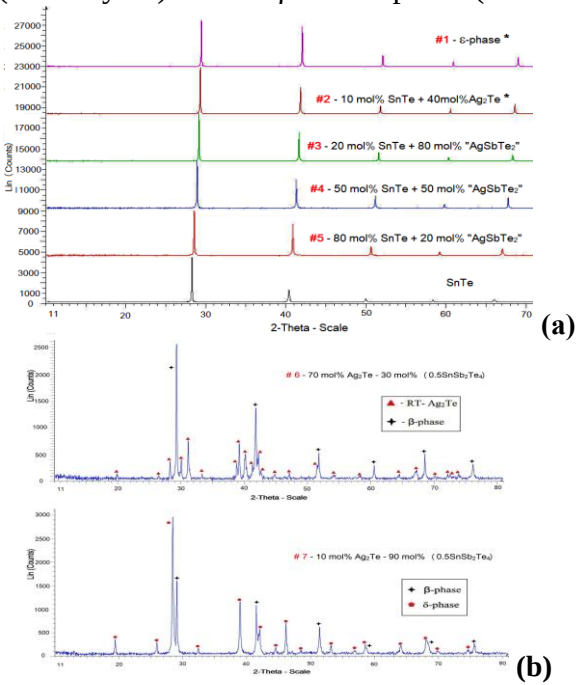

Fig. 16. Powder X-ray diffraction patterns of selected alloys #1-5 (a) and #6 and #7 (b) in Fig. 12 [22]. *Alloys hardened from 700 K

Projection of the liquidus surface. The liquidus surface (Fig. 17) consists of five fields corresponding to the primary crystallization of the α′-, α-, β-, and γ-phases based on HT-Ag_2Te, IT-Ag_2Te, SnTe, and Sb_2Te_3, as well as the δ-phase based on the ternary compound $SnSb_2Te_4$. The largest crystallization field in the system belongs to the β-phase (field 3 in Fig. 17). The fields of primary crystallization of the phases are limited by peritectic (p_1U) and eutectic (e_2e_3, e_1U, Up_2) curves (Fig. 17). The types and temperatures of all non- and monovariant equilibria in the Ag_2Te-SnTe-Sb_2Te_3 system are given

in the dissertation.

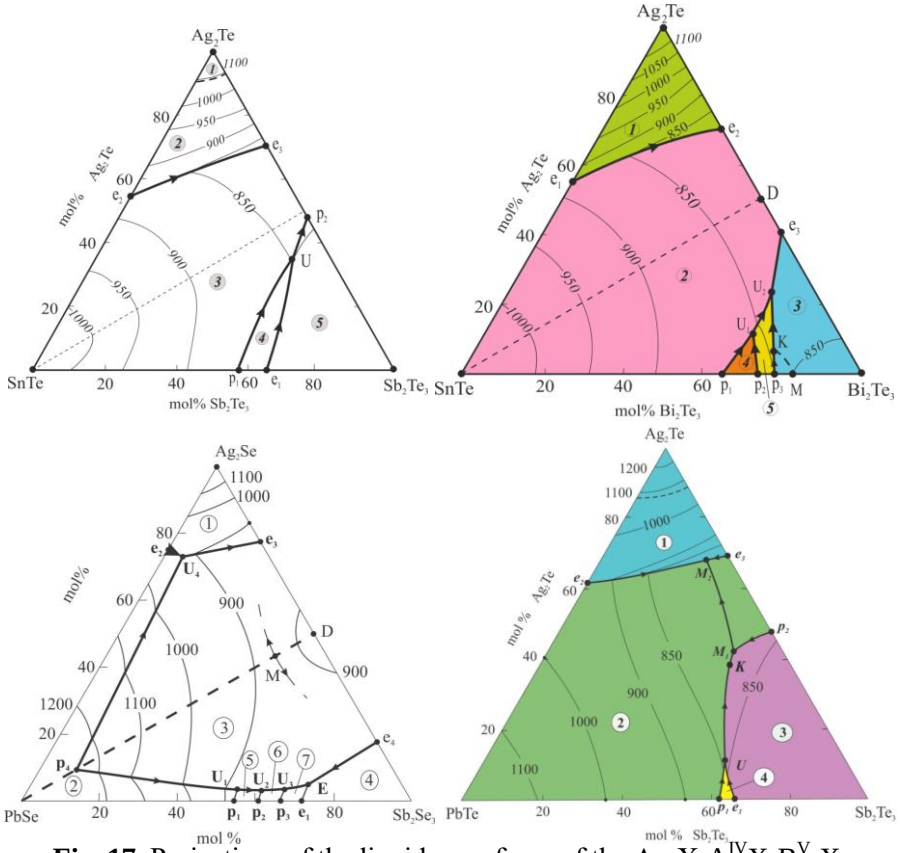

Fig. 17. Projections of the liquidus surfaces of the Ag_2X-$A^{IV}X$-$B^{V}_2X_3$ systems [21, 22, 35, 38]. Fields of primary crystallization of the **system Ag_2Te-SnTe-Sb_2Te_3**: **1**, α´; **2**, α; **3**, β; **4**, δ; **5**, γ [22]; **system Ag_2Te-SnTe-Bi_2Te_3**: **1,** α; **2,** γ; **3,** β; **4,** $SnBi_2Te_4$; **5,** $SnBi_4Te$; **system Ag_2Se-PbSe-Sb_2Se_3**: **1** - α; **2** - β_1; **3** - γ; **4** - β_2; **5** - $Pb_2Sb_2Se_5$; **6** - $Pb_4Sb_6Se_{13}$; **7** - $PbSb_2Se_4$ [35]; **Ag_2Te-PbTe-Sb_2Te_3 system: 1**- α (α´)**; 2** - β**; 3** - γ**; 4** - $Pb_2Sb_6Te_{11}$ [38]

SnTe-"$AgSbTe_2$" section. Four polythermal sections, which almost completely intersect the quasi-ternary system under study, were studied in the context of the liquidus surface projection. Here, we will consider only SnTe-"$AgSbTe_2$". This section is characterized

by the formation of a wide (~85 mol%) solid solution based on SnTe (Fig. 18). The liquidus and solidus temperatures decrease monotonically from the melting point of pure SnTe (1080 K) to 860 K. Three series of thermal effects were observed in the DTA heating curves of alloys with <15 mol.% SnTe, subjected to prolonged annealing at 700 K and subsequent additional annealing at 400 K. In addition to the main peaks at 840-860 K, weak thermal effects were detected at 815-830 K and at 415 K.

Comparison with Fig. 18 shows that in these alloys, after the primary crystallization of the β-phase, a monovariant crystallization of the eutectic mixture α+β occurs (curve e_2e_3). Thermal effects at 415 K correspond to the nonvariant eutectoid equilibrium α→RT-Ag_2Te+β+γ. Thermal effects at 630 K, corresponding to the decomposition of the ε-phase into the α-phase and Sb_2Te_3 in SnTe-"$AgSbTe_2$" alloys, were not detected. The phase regions α+β, α+β+γ, and RT-Ag_2Te+β+γ are delimited by dashed lines. The narrow two-phase regions α+γ and RT-Ag_2Te+γ, the extent of which could not be determined experimentally, are also shown by dashed lines in Fig. 18.

Ag_2Te-SnTe-Bi_2Te_3 system. In Section 4.2 of the dissertation, the phase relations in the Ag_2Te-SnTe-Bi_2Te_3 system are experimentally investigated. Five polythermal sections of SnTe-$AgBiTe_2$, Ag_2Te-$0{,}5SnBi_2Te_4$, [AgSn0,5Te]-$AgBiTe_2$, $0{,}5SnBi_2Te_4$-$AgBiTe_2$ and [$AgSn_{0.5}Te$]-Bi_2Te_3, two isothermal sections at 300 and 800 K, as well as a projection of the liquidus surface of the system, are constructed.

Quasi-binary section of SnTe-$AgBiTe_2$. The phase diagram of the SnTe-$AgBiTe_2$ system is partially quasi-binary (above 715 K) and is characterized by the formation of a continuous series of high-temperature solid solutions (γ-phases) based on both parent compounds (Fig. 18). These solid solutions crystallize in a cubic NaCl-type structure and are isostructural to known thermoelectric materials in the $AgSbTe_2$-PbTe system.

Two thermal effects were detected below the solidus in the differential thermal analysis (DTA) curves of alloys containing 70-100 mol% $AgBiTe_2$. We hypothesize that the thermal effects at 640-715 K are due to the solid-state decomposition of the high-

temperature γ-phase into the IT-Ag_2Te-based α-phase and the Bi_2Te_3-based β-phase, respectively. The thermal effects at 410 K correspond to the α↔LT-Ag_2Te polymorphic transition.

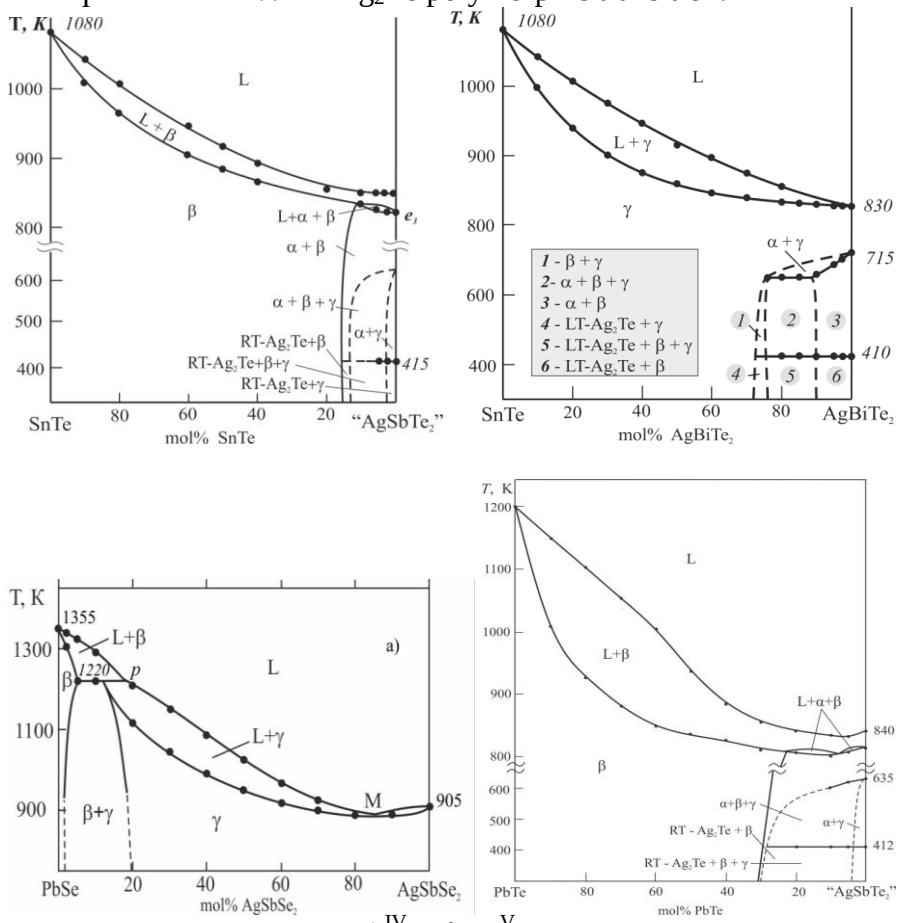

Fig. 18. Phase diagrams of the $A^{IV}X$-$AgB^{V}X_2$ type systems [21, 22, 32,38]

Solid-phase equilibria. *Isothermal section at 800 K.* As can be seen from Fig. 15, the homogeneity region of the γ-phase is quite wide on both sides of the SnTe-$AgBiTe_2$ section and continuously narrows toward $AgBiTe_2$. At this temperature, a wide two-phase region α+γ is formed between the γ- and α-phases (Fig. 15), which completely encompasses the SnTe-Ag_2Te-$AgBiTe_2$ subsystem.

The general scheme of solid-phase equilibria in the $SnTe$-Bi_2Te_3-$AgBiTe_2$ subsystem is more complex. Here, the γ-phase forms three two-phase (γ+$SnBi_2Te_4$, γ+$SnBi_4Te_7$, β+γ) and two three-phase (γ+$SnBi_2Te_4$+$SnBi_4Te_7$, γ+$SnBi_4Te_7$+$SnBi_6Te_{10}$) regions with mixed-layer phases of the tetradymite type of the $SnTe$-Bi_2Te_3 system.

Isothermal section at 300 K (Fig. 15) exhibits slightly different solid-phase equilibria. Decomposition of the γ-phase in the region >70 mol.% $AgBiTe_2$ (Fig. 15) leads to a narrowing of the LT-Ag_2Te+γ, γ+$SnBi_4Te_7$, and γ+β phase regions and the formation of a broad three-phase LT-Ag_2Te+β+γ and a two-phase LT-Ag_2Te+β region.

The liquidus surface projection (Fig. 17) consists of three fields corresponding to the primary crystallization of the α-, β-, and γ-phases, as well as the ternary compounds $SnBi_2Te_4$ and $SnBi_4Te_7$. The largest crystallization field in the system belongs to the γ-phase (field 2 in Fig. 17). The primary crystallization fields of the phases are bounded by peritectic (p_1U_1, p_2U_1, p_3K) and eutectic(e_1e_2, U_1U_2, U_2e_3, KU_2) curves (Fig. 17). The curve from the minimum point (M) connects with the peritectic curve from the p_3 peritectic (point K) and transforms into the eutectic curve KU_2.

The Ag_2Se-$PbSe$-Sb_2Se_3 system was studied over its entire concentration range (Section 4.3 of the dissertation).

The $PbSe$-$AgSbSe_2$ quasi-binary section belongs to the peritectic type (Fig. 18). The peritectic has coordinates of 18 mol% $AgSbSe_2$ and 1220 K. The solubility of $AgSbSe_2$ and $PbSe$ at the peritectic temperature is 87 (γ-phase) and 5 mol% (β-phase), and at room temperature, 80 and 2 mol%, respectively. A minimum point (M) is observed on the liquidus and solidus curves.

Solid-phase equilibria at 300 K. The solid-phase equilibria diagram (Fig. 19) shows that a characteristic feature of the Ag_2Se-$PbSe$-Sb_2Se_3 system is the presence of a wide solubility field based on $AgSbSe_2$. This field (γ) has the form of a band with a length of 80 mol.% along the quasi-binary section $PbSe$-$AgSbSe_2$, and its width expands in the direction of $AgSbSe_2$, reaching 12-13 mol.%.

The solubility of $PbSe$-based compounds is approximately 2-3 mol%. γ-solid solutions play a decisive role in the formation of phase fields in the system. They form junctions with all other phases,

resulting in the formation of a series of two-phase and three-phase regions.

Isothermal section at 900 K. The phase diagram (Fig. 19) consists primarily of a liquid phase and two- and three-phase regions with the presence of liquid. Using this phase diagram, single crystals with α, β_1 compositions and, in particular, γ-solid solutions of a given composition can be grown, taking into account the direction of the tie lines in the two-phase regions.

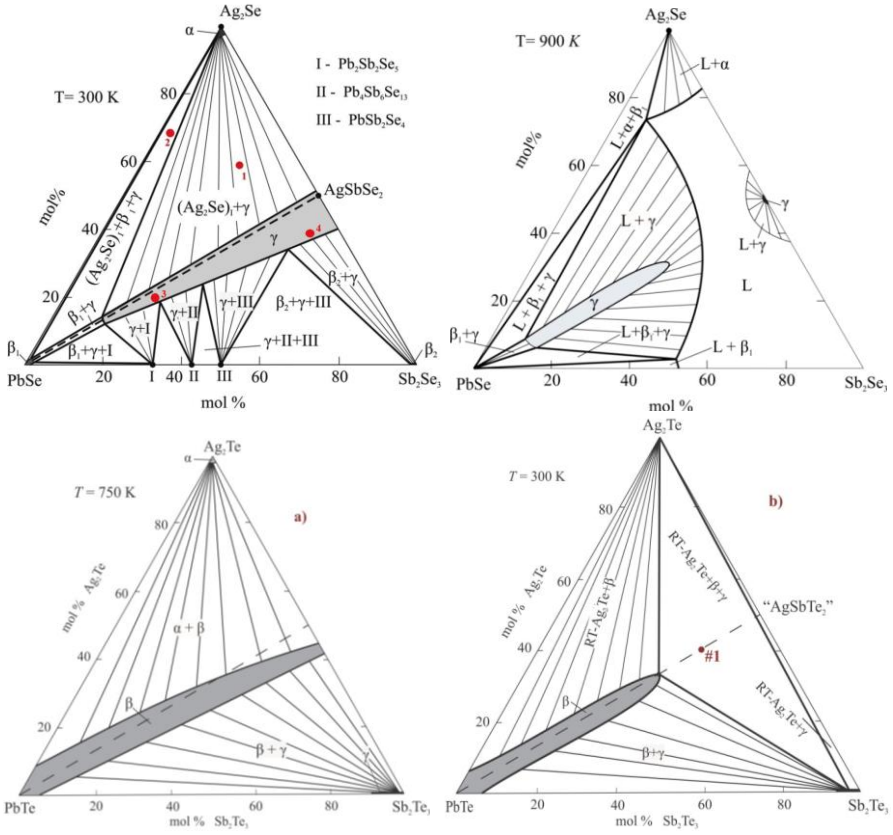

Fig. 19. Isothermal sections of the phase diagram of the Ag_2Se-PbSe-Sb_2Se_3 [29] and Ag_2Te-PbTe-Sb_2Te_3 [38] systems

The liquidus surface of the Ag_2Se-PbSe-Sb_2Se_3 system consists of seven primary crystallization regions (Fig. 17). The largest area in the system belongs to the primary crystallization surface belonging to the γ-phase. This phase crystallizes directly from solution in the temperature range of 908-1020 K.

These liquidus surfaces are bounded by 12 monovariant equilibrium curves and 13 invariant points.

Ag_2Te-PbTe-Sb_2Te_3 system. Section 4.4 presents the liquidus surface projection of the system, isothermal sections at 750 K and 300 K, and five vertical sections of the phase diagram of this system.

The PbTe-"$AgSbTe_2$" section is characterized by the formation of broad (up to 70 mol%) solid solutions based on PbTe (β-phase), but the system as a whole is not quasi-binary (Fig. 18). This is because the starting component "$AgSbTe_2$" is not an individual compound, but a two-phase alloy $Ag_2Te+Ag_{1-x}Sb_{1+x}Te_{2+x}$.

X-ray diffraction results confirmed the formation of a solid solution with a cubic structure in a wide region (30-100 mol.% PbTe) in the studied cross-section. Alloys with low PbTe content are three-phase.

Isothermal section at 750 K. In the Ag_2Te-PbTe-Sb_2Te_3 system, a wide (up to 8 mol.%) continuous band of β-solid solution is formed at 750 K (Fig. 19). The width of β-solid solutions is 3-4 mol.% along the Ag_2Te-Sb_2Te_3 section and expands to 7-8 mol.% when the composition changes towards PbTe. The PbTe-" $Ag_{0.84}Sb_{1.16}Te_{2.16}$" section is entirely within the homogeneity region of the β-phase. The PbTe-"$AgSbTe_2$" region in the composition range of 25-100 mol.% PbTe passes through the homogeneity region of the β-phase, and at <25 mol.% PbTe it transitions to the two-phase region α+β. The β-phase forms tie lines with the α-phase and γ-phase.

Solid-phase equilibria at 300 K (Fig. 19). At temperatures below 635 K, the decomposition of the intermediate phase $Ag_{1-x}Sb_{1+x}Te_{2+x}$ leads to partial decomposition of the β-phase in the composition range <25 mol.% PbTe and the formation of the following heterogeneous regions: RT-Ag_2Te+β+γ and RT-Ag_2Te+γ.

The projection of the liquidus surface of the Ag_2Te-PbTe-Sb_2Te_3 system consists of 4 fields corresponding to the primary

crystallization of the α-, β-, and γ-phases, as well as the ternary compound $Pb_2Sb_6Te_{11}$ (Fig. 17). The region of primary crystallization of the α-phase is delimited from the α′-phase based on HT-Ag_2Te by a dashed line. The largest crystallization field in the system belongs to the β-phase (field 2 in Fig. 17). This region is divided into 2 parts by the curve M_1M_2, connecting the M_1 and M_2 minimum points. The region of primary crystallization of the ternary compound $Pb_2Sb_6Te_{11}$ is very small (field 4 in Fig. 17).

The transition equilibrium U limits the extent of this region within the concentration triangle. This is in good agreement with the data on the narrow temperature range of the $Pb_2Sb_6Te_{11}$ compound. The primary crystallization regions of the phases are bounded by peritectic (p_1U, p_2M_1) and eutectic (e_2M_2, M_2e_3, e_1U, UM_1) curves (Fig. 27). The types and temperatures of all invariant and monovariant equilibria in the Ag_2Te-SnTe-Sb_2Te_3 system are presented in the dissertation.

Features of phase equilibria in the $A^{IV}X$-$AgB^{V}X_2$ systems

A characteristic feature of all these systems is the formation of a continuous series of solid solutions between the parent compounds or broad regions of solid solutions based on them. This is because the parent compounds or certain crystalline modifications of them are isostructural.

From the literature review cited in the dissertation, it follows that all tin and lead monochalcogenides crystallize in a cubic NaCl-type structure, or at least one of their crystalline modifications belongs to this structural type. On the other hand, ternary $AgB^{V}X_2$ compounds also typically exhibit a cubic NaCl-type structure.

A comparison of the phase diagrams of $A^{IV}X$-$AgB^{V}X_2$ type systems (Fig. 18) revealed that:

1) Both selenide systems (PbSe-$AgSbSe_2$ and PbSe-$AgBiSe_2$) are quasi-binary. The first belongs to the peritectic type with limited mutual solubility of the initial compounds, despite their isostructurality. This is apparently due to the relatively large difference in the lattice parameters (a = 6.1243 Å (PbSe); a = 5.786 Å ($AgSbSe_2$) and a=7.245 Å ($AgBiSe_2$)), as well as to the nature of

the chemical bond in the initial compounds. PbSe has predominantly ionic bonding, while in $AgSbSe_2$ the proportion of covalency is significantly higher. The second section of this type is characterized by the formation of a continuous series of solid solutions between PbSe and the high-temperature cubic modification of $AgBiSe_2$. The formation of the γ-phase is accompanied by a sharp decrease in the temperature of the polymorphic transition of $AgBiSe_2$ (590 K) and stabilization of the cubic modification of solid solutions at room temperature.

2) The SnTe-$AgBiTe_2$ and PbTe-$AgBiTe_2$ systems are partially quasi-binary and are characterized by the formation of a continuous series of substitutional solid solutions. In both systems, decomposition of solid solutions and violation of the quasi-binarity conditions are observed near $AgBiTe_2$. This phenomenon is because the $AgBiTe_2$ compound exists in a narrow temperature range (715-830 K) and at 715 K decomposes into Ag_2Te and Bi_2Te_3. A more detailed description of the influence of this phenomenon on the nature of the phase equilibria of these systems is given below.

3) The SnTe-"$AgSbTe_2$" and PbTe-"$AgSbTe_2$" systems are non-quasi-binary and are characterized by the formation of broad homogeneity regions based on tin and lead tellurides. This is because in the Ag_2Te-Sb_2Te_3 system, the stoichiometric compound $AgSbTe_2$ is absent, and the intermediate phase with a cubic structure has a composition richer in antimony.

Thus, in the systems considered, especially in the telluride systems, the nature of phase equilibria is highly temperature-dependent. This is more clearly demonstrated by a comparison of solid-phase equilibrium diagrams at different temperatures, which are discussed below.

Features of solid-phase equilibria in the Ag_2X-$A^{IV}X$-$B^{V}{}_2X_3$ systems

Solid-phase equilibria at relatively high temperatures. Figs. 15 and 19 show isothermal sections of the phase diagrams of some Ag_2X-$A^{IV}X$-$B^{V}{}_2X_3$ systems at various temperatures in the range 700-900 K.

These phase diagrams clearly demonstrate the formation of continuous solid solutions along or near the $A^{IV}X$-$AgB^{V}X_2$ sections. These homogeneity regions appear as wide bands on either side of

the composition lines of these sections. An exception is the Ag_2Se-$PbSe$-Sb_2Se_3 system, in which the band of the γ-phase homogeneity region is not continuous and should be considered a solid solution based on $AgSbSe_2$. A relatively narrow region of solid solutions exists based on PbSe.

A comparison of the phase diagrams shows that in three systems, namely Ag_2Se-$PbSe$-Bi_2Se_3, Ag_2Te-$SnTe$-Bi_2Te_3, and Ag_2Te-$PbTe$-Bi_2Te_3, the $A^{IV}X$-$AgB^{V}X_2$ sections are entirely within the solid solution bands. At the same time, in the Ag_2Te-$SnTe$-Sb_2Te_3 и Ag_2Te-$PbTe$-Sb_2Te_3 systems, in the region of compositions rich in silver and antimony, the homogeneity bands deviate from the $A^{IV}Te$-"$AgSbTe_2$" sections toward the ε-phase with a cubic structure of the Ag_2Te-Sb_2Te_3 boundary system. As a result, the alloys near the imaginary "$AgSbTe_2$" compound are located in two-phase regions and contain the α-phase based on Ag_2Te.

Another feature of the high-temperature solid-phase equilibria in the systems under consideration should be noted. As can be seen from the solid-phase equilibria figures, the silver-saturated solid solution compositions in all of them are in a connodal relationship with Ag_2Se or Ag_2Te. At the same time, different phase equilibria are observed in the lower parts of the concentration triangles. In most systems, the boundary quasi-binary components $A^{IV}X$-$B^{V}{}_2X_3$ form tetradymite-like ternary compounds. These, like the phases based on binary compounds $B^{V}{}_2X_3$ form stable connodes with the limiting compositions of the solid solution bands. An exception is the Ag_2Te-$PbTe$-Sb_2Te_3 system, in which the side system does not form ternary compounds stable at this temperature.

Figs.15 and 19 also show solid-phase equilibria diagrams of the Ag_2X-$A^{IV}X$-$B^{V}{}_2X_3$ systems at room temperature. As can be seen, significant changes occur in all the systems considered compared to the diagrams at 700-900 K. The most significant changes are observed in the thalluride systems. This is due to the solid-phase decomposition of ternary phases ($AgBiTe_2$ and the ε-phase near $AgSbTe_2$) of the Ag_2Te-SnTe (PbTe) boundary systems. As a result of these processes, two- and three-phase regions are formed in the phase diagrams, involving the low-temperature (room-temperature)

modification of Ag_2Te and $B^V_2Te_3$-based phases. These heterogeneous regions encompass the $A^{IV}X$-AgB^VX_2 sections, disrupting their stability.

Comparison of liquidus surfaces of the Ag_2X-$A^{IV}X$-$B^V_2X_3$ systems

A comparison of the liquidus surface projections of the systems under consideration shows (Fig. 17) that in all of them, the primary crystallization fields of solid solutions along the $A^{IV}X$-AgB^VX_2 sections occupy a significantly larger fraction of the concentration triangle area than all other phases combined, i.e., they are the dominant phases in these systems.

Four of the six $A^{IV}X$-AgB^VX_2 systems are quasi-binary in the high-temperature region of the T-x-y diagrams. The exceptions are the Ag_2Te-$SnTe$-Sb_2Te_3 and Ag_2Te-$PbTe$-Sb_2Te_3 systems, in which the $AgSbTe_2$ compound is absent.

Phase Equilibria in the Cu_3SbS_4-GeS_2 and Cu_3SbSe_4-$GeSe_2$ systems. Chapter 4 also presents the results of a study of the Cu_3SbS_4-GeS_2 and Cu_3SbSe_4-$GeSe_2$ systems. The aim is to obtain and characterize new phases of variable composition with Sb↔Ge substitution based on the Cu_3SbS_4 and Cu_3SbSe_4 phases, which are synthetic analogs of the mineral famatinite and exhibit high thermoelectric properties.

It was established that Cu_3SbSe_4-$GeSe_2$ samples containing no more than 15 mol% $GeSe_2$ are single-phase and exhibit diffraction peaks identical to those of pure Cu_3SbSe_4, with a slight shift to the right (Fig. 20).

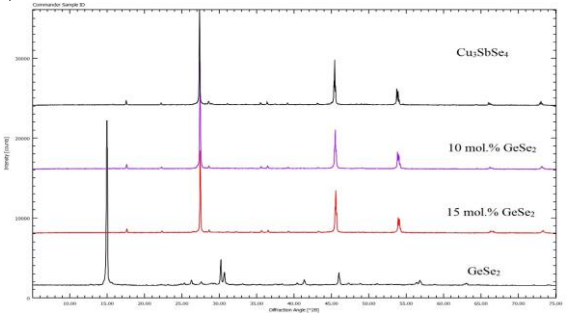

Fig. 20. Powder diffraction patterns of alloys Cu_3SbSe_4-$GeSe_2$ [43]

This indicates the formation of up to 15 mol% solid solutions

based on the Cu_3SbSe_4 compound, which is also confirmed by the DTA results (Fig. 21). However, the Cu_3SbSe_4-$GeSe_2$ system as a whole is non-quasi-binary and is characterized by a complex interaction pattern. The DTA data for alloys with a high $GeSe_2$ content could not be interpreted. Therefore, Fig. 21 shows a fragment of the phase diagram of the Cu_3SbSe_4-$GeSe_2$ system.

XRD analysis showed that in the composition range of 15-58 mol% $GeSe_2$, the alloys consist of a Cu_3SbSe_4+Cu_2GeSe_3+Sb_2Se_3+Se

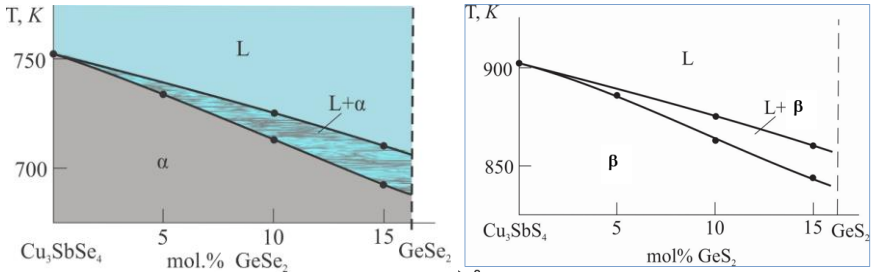

Fig. 21. Fragments of phase diagrams of systems Cu_3SbS_4-GeS_2 and Cu_3SbSe_4-$GeSe_2$ [43]

four-phase mixture. The alloy with a composition of 60 mol% $GeSe_2$ is three-phase: Cu_2GeSe_3+Sb_2Se_3+Se. Alloys containing more than 60 mol% $GeSe_2$ consist of a Cu_2GeSe_3+Sb_2Se_3+$GeSe_2$+Se four-phase mixture. Based on the obtained data, it can be concluded that the Cu_3SbSe_4-$GeSe_2$ section is located in the four-phase regions Cu_3SbSe_4+ Cu_2GeSe_3+Sb_2Se_3+Se (region 1 in Fig. 27) and Cu_2GeSe_3+Sb_2Se_3+$GeSe_2$+Se (region 2 in Fig. 22) of the Cu_2Se-$GeSe_2$-Sb_2Se_3-Se concentration tetrahedron. These regions are delimited by the stable Cu_2GeSe_3-Sb_2Se_3-Se concentration triangle. The alloy with the composition located on the plane of this triangle corresponds to 60 mol.% $GeSe_2$ (point A in Fig. 22).

A similar picture is observed in the Cu_3SbS_4-GeS_2 system (Fig. 21 and 22).

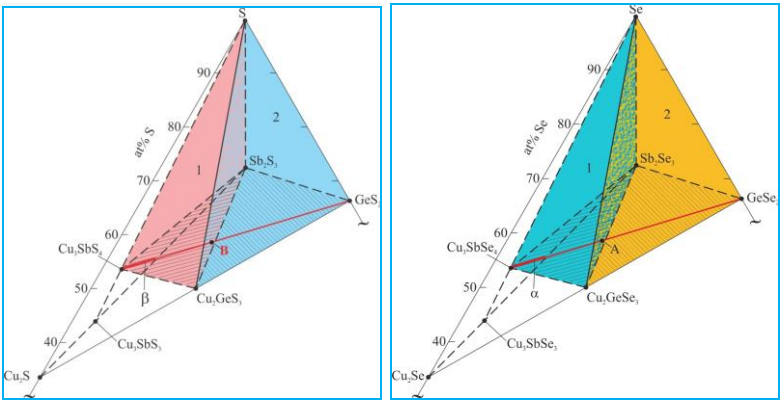

Fig. 22. Concentration tetrahedres Cu_2S-GeS_2-Sb_2S_3-S and Cu_2Se-$GeSe_2$-Sb_2Se_3-Se [43]

Chapter 5 presents the results of a thermodynamic study of the ternary systems Cu-As-S, Cu-As-Se, Cu-Sb-S, Ag-As-S, Ag-As-Se, and Ag-Sb-Se. For the first three systems, we obtained new, refined phase equilibria, including complete T-x-y diagrams and their various poly- and isothermal cross-sections (see Chapter III). For the remaining three systems, the nature of solid-phase equilibria was established, and the corresponding data were used to plan EMF experiments and process their results. The research results are presented in [1, 2, 4-6, 10, 28, 34, 41, 42, 46-49, 52].

Chapter 5 begins with a brief description of the EMF method with solid cation-conducting and liquid electrolytes, as well as the specifics of its application to heterogeneous systems (Section 5.1). The methods for planning and conducting experiments, as well as processing their results (Section 5.2), are outlined. The following sections present and discuss results for specific systems.

Thermodynamic properties of copper-arsenic sulfides

For the thermodynamic study of the Cu-As-S system, the following concentration cells were assembled

(-) Cu (s.) | $Cu_4RbCl_3I_2$ (s) | (Cu+ in alloys) (s) (+) (**1**)

The compositions of the alloys - the right electrodes of the circuits of type (1), as well as the conditions of their synthesis and thermal annealing, were selected based on our data on solid-phase equilibria

in the Cu-As-S system (Fig. 1).

To calculate the thermodynamic functions of ternary compounds I-IV (Fig. 1), the data on EMF measurements in the Cu_3AsS_4+As_2S_3+S, Cu_3AsS_4+$Cu_6As_4S_9$+As_2S_3, Cu_3AsS_4+$Cu_{12}As_4S_{13}$+$Cu_6As_4S_9$, $Cu_6As_4S_9$+CuAsS+AsS three-phase regions, respectively, were used. The temperature dependences of the EMF of cells of type (1) were constructed for a number of the above-mentioned phase regions of the Cu-As-S system (Fig. 23). As can be seen, all these dependences are linear and can be used in thermodynamic calculations.

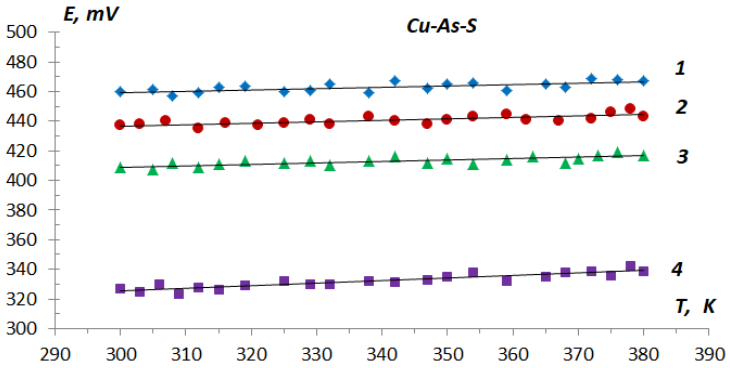

Fig. 23. Temperature dependences of the EMF of cells of type (1) for alloys of the Cu-As-S system from phase regions Cu_3AsS_4+As_2S_3+S (**1**), Cu_3AsS_4+$Cu_6As_4S_9$+As_2S_3 (**2**), Cu_3AsS_4+$Cu_{12}As_4S_{13}$+$Cu_6As_4S_9$ (**3**), $Cu_6As_4S_9$+CuAsS+AsS (**4**) [47]

The results of EMF measurements in these phase regions were processed using the least squares method, and linear equations of the type

$$E, mV = a + bT \pm 2S_E(T) \quad (2)$$

were obtained. From these equations of temperature dependences of EMF (Table 3) according to the relations

$$\Delta\bar{G}_{Cu} = -nFE \quad (3)$$

$$\Delta\bar{S}_{Cu} = zF\left(\frac{\partial E}{\partial T}\right)_P = zFb \quad (4)$$

$$\Delta\bar{H}_{Cu} = -zF\left[E - T\left(\frac{\partial E}{\partial T}\right)_P\right] = -zFa \quad (5)$$

(z is the charge of the potential-forming cation Cu^+, F is the Faraday number, a and b are constants in the equation E=a+bT), the relative partial thermodynamic functions of copper in alloys at 298 K were calculated (Table 4).

According to Fig. 1, the values of the molar partial quantities in the above three-phase regions are thermodynamic characteristics of the following potential formation reactions (the state of all substances is crystalline):

$$3Cu+0.5As_2S_3+2.5S=Cu_3AsS_4 \quad (6)$$

$$2\tfrac{4}{7}Cu + 2\tfrac{2}{7}Cu_3AsS_4 + \tfrac{3}{7}Cu_6As_4S_9 = Cu_{12}As_4S_{13} \quad (7)$$

$$2.4Cu + 1.2Cu_3AsS_4 + 1.4As_2S_3 = Cu_6As_4S_9 \quad (8)$$

$$Cu+AsS=CuAsS \quad (9)$$

Equations (6)–(9) made it possible to calculate the standard thermodynamic functions of formation and the standard entropies of the corresponding ternary phases (Table 5).

Thermodynamic studies of the Cu-As-Se and Cu-Sb-S systems were carried out in a similar way. The standard thermodynamic functions of formation and the standard entropies of the ternary phases formed in them are given in Table 5. The dissertation provides a comparative analysis of the experimental results obtained [6, 41, 47, 52] with literature data.

Table 3.

Temperature dependences of the EMF of cells of type (1) in some phase regions of the Cu-As-S system (T=300-380K) [47]

Phase area in Fig.1	E, mV=a+вT±2S_E(T)
I+As_2S_3+S	$432{,}4+0{,}092T\pm 2\left[\frac{4{,}5}{20}+6\cdot10^{-5}(T-339{,}1)^2\right]^{1/2}$
I+III+As_2S_3	$415{,}6+0{,}073T\pm 2\left[\frac{7{,}8}{21}+8\cdot10^{-5}(T-341{,}6)^2\right]^{1/2}$
I+II+III	$378{,}2+0{,}102T\pm 2\left[\frac{8{,}3}{21}+8\cdot10^{-5}(T-341{,}8)^2\right]^{1/2}$
III+IV+AsS	$284{,}6+0{,}142T\pm 2\left[\frac{6{,}1}{22}+7\cdot10^{-5}(T-341{,}9)^2\right]^{1/2}$

Table 4.

Partial molar functions of copper in Cu-As-S alloys at 298 K [47]

Phase area in Fig.1	$-\Delta\overline{G}_{Cu}$	$-\Delta\overline{H}_{Cu}$	$\Delta\overline{S}_{Cu}$,
	kJ·mol^{-1}		J·mol^{-1}·K^{-1}
I+As_2S_3+S	44.37±0.11	41.72±0.51	8.9±1.5
I+III+As_2S_3	42.20±0.13	40.10±0.60	7.0±1.7
I+II+III	39.43±0.13	36.49±0.61	9.8±1.7
III+IV+AsS	31.55±0.12	24.46±0.56	13.7±1.6

Table 5.

Standard thermodynamic functions of formation and standard entropies of ternary phases of the Cu-As-S, Cu-As-Se, and Cu-Sb-S systems [6, 41, 47, 52]

Compound	$-\Delta_f G^0(298K)$	$-\Delta_f H^0(298K)$	$S^0(298K)$,
	κJ·mol^{-1}		J·K^{-1}·mol^{-1}
Cu_3AsS_4	179,2±0,6	172,2±2,6	278±8
$Cu_6As_4S_9$	445,3±1,6	434,6±7,5	668±22
$Cu_{12}As_4S_{13}$	701,8±2,5	673,7±10,7	1050±13
CuAsS	69,5±0,3	64,1±1,7	109±5
Cu_3AsSe_4	147.3±0.5	146.3±1.5	307±13
$Cu_7As_6Se_9$	441,8±2,3	446,1±11,7	970±27
$CuAsSe_2$	61.1±0.4	62.1±1.9	149.5±4.5
Cu_3AsSe_3	141,8±0,5	140,0±2,0	258,5±5,6
CuAsSe	55,1±0,3	55,6±2,0	109,5±4,7
Cu_3SbS_4	254.7 ± 2.3	247.8 ± 2.3	295.6 ± 7.0
$CuSbS_2$	128.5 ± 2.2	126.9 ± 2.4	147.5 ± 3.8
$Cu_{12}Sb_4S_{11}$	958.7 ± 9.6	929.7 ± 11.2	1092.0 ± 29.0
Cu_3SbS_3	226.4 ± 2.3	219.0 ± 2.6	265.5 ± 7.2
$Cu_{14}Sb_4S_{13}$	971.7 ± 9.8	984.8 ± 11.9	1018.0 ± 33.0

Section 5.4 presents the results of a study of the Ag-As-S(Se) and Ag-Sb-Se systems using the EMF method with a solid Ag^+ conducting electrolyte Ag_4RbI_5 in the temperature range of 300-380 K. For each of the three systems, solid-phase equilibrium diagrams were initially constructed, which reflected the ternary compounds formed in them

(Fig. 24).

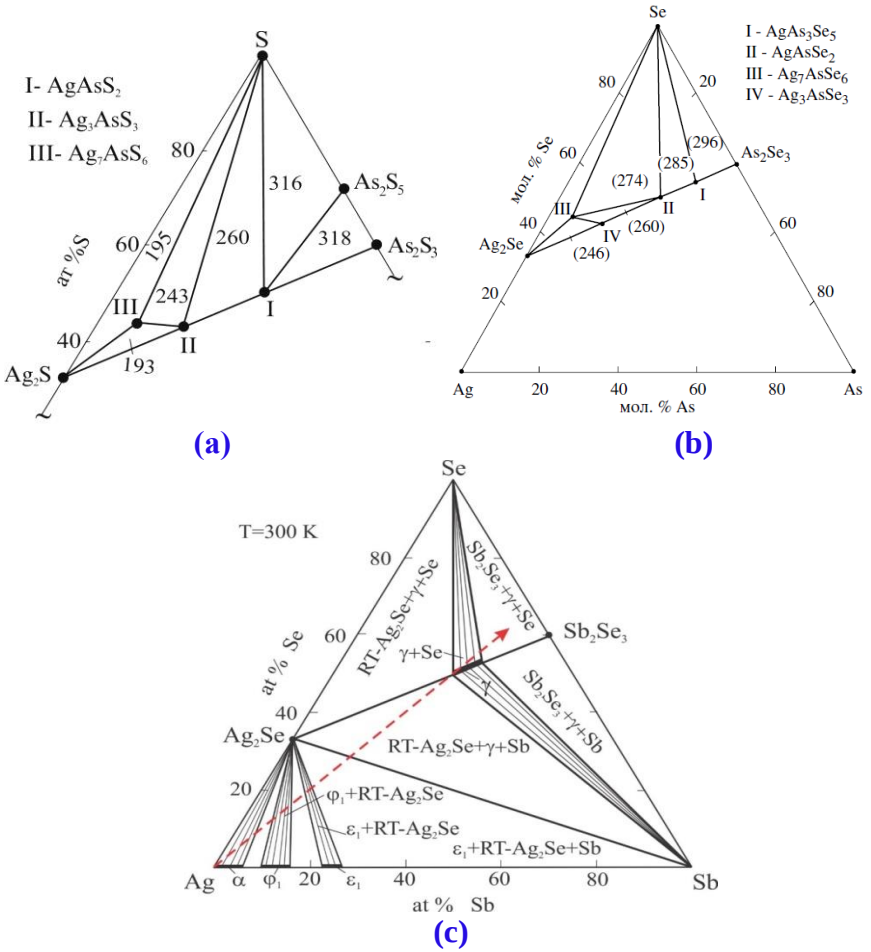

Fig. 24. Solid-phase equilibria diagrams (300 K) of the systems Ag_2S-As_2S_3-S **(a),** Ag_2Se–As_2Se_3–Se **(b),** and Ag-Sb-Se **(c)** [1, 10, 42]

As can be seen from Figure 24, three ternary compounds are formed in the Ag-As-S system: $AgAsS_2$, Ag_3AsS_3, and Ag_7AsS_6. In the Ag-As-Se system, we confirmed the existence of four ternary compounds: $AgAs_3Se_5$, $AgAsSe_2$, Ag_3AsSe_3, and Ag_7AsSe_6. The system is characterized by the formation of a single compound,

$AgSbSe_2$, which forms the basis for solid solutions along the Ag_2Se-Sb_2Se_3 section. For the study, concentration cells of the following type were compiled:

(-) Ag (s) / Ag_4RbI_5(s) / (Ag in alloys) (s) (+) (10)

The studies and calculations were conducted similarly to those for copper-based ternary systems. From the measured EMF data for concentration cells of type (10) in the above-mentioned systems, linear equations for the temperature dependences of EMF were derived, from which partial molar functions of silver were calculated in certain phase regions of these systems.

Next, using these values, the standard thermodynamic functions of formation and standard entropies of ternary compounds and two phases of variable composition in the Ag-As-S(Se) and Ag-Sb-Se systems were calculated.

Table 6.

Standard integral thermodynamic functions of ternary compounds of systems Ag-As-S, Ag-As-Se и Ag-Sb-Se [1, 10, 42]

Compound	$-\Delta_f G^0(298K)$	$-\Delta_f H^0(298K)$	$S^0(298K)$
	кJ·mol^{-1}		J·mol^{-1}·K^{-1}
$AgAsS_2$	77,9±0,4	75,69±1,6	151±5
Ag_3AsS_3	128,2±0,6	121,4±2,8	283±10
Ag_7AsS_6	222,0±1,2	201,9±6,0	594±19
$AgAs_3Se_5$	111,9±10,5	112,5±0,5	359,1±7,5
$AgAsSe_2$	55,6±3,6	54,4±3,5	167,0±3,8
Ag_7AsSe_6	214±4,2	199,5±6,5	637±16
Ag_3AsSe_3	107,8±3,8	101,8±4,6	310,7±7,7
$Ag_{0.8}Sb_{1.2}Se_{2.2}$	96.0±1.8	98.6±0.9	183.8±2.5
$Ag_{0.9}Sb_{1.1}Se_{2.1}$	93.8±1.8	97.0±1.0	179.6±2.5
$AgSbSe_2$	91.4±1.5	93.5±1.0	174.6±2.4

The obtained standard thermodynamic functions of formation and standard entropies of ternary phases of the Ag-As-S, Ag-As-Se, and Ag-Sb-Se systems are given in Table 6. The dissertation contains a comparative analysis of the obtained thermodynamic functions for some compounds [1, 10, 42] with available literature data.

In Chapter 6, the thermodynamic properties of solid solutions in the Ag_2X-$A^{IV}X$-$B^{V}{}_2X_3$ systems were studied along the $A^{IV}X$-$AgB^{V}X_2$ sections. Two modifications of the EMF method were used: with a solid Ag^+-conducting electrolyte and a liquid glycerol electrolyte. The results of these studies are presented in [8, 9, 15, 18, 20-22, 25-27, 30, 37-39].

The Ag_2Te-$SnTe$-Sb_2Te_3, Ag_2Te-$SnTe$-Bi_2Te_3, and Ag_2Te-$PbTe$-Sb_2Te_3 systems were studied by the EMF method with the Ag_4RbI_5 solid electrolyte in the temperature range of 300-430 K and using electrochemical cells of the (10) type. In the studied systems, the formation of wide (≥80 mol% $AgB^{V}Te_2$) regions of solid solutions along the Sn(Pb)Te-AgSb(Bi)Te_2 sections was confirmed. The partial thermodynamic functions of silver in the alloys were calculated from the equations of the temperature dependences of the EMF. Based on literature data on solid-phase equilibria in Ag_2X-$A^{IV}X$-$B^{V}{}_2X_3$ systems, potential-forming reactions were determined, which were used to calculate the standard thermodynamic functions of formation and the standard entropies of the $(2A^{IV}X)_x(AgB^{V}X_2)_{1-x}$ solid solutions. The obtained values for all three quasi-binary systems studied are presented in Table 7.

Thermodynamic studies of the Ag_2Te-$PbTe$-Sb_2Te_3 and Ag_2Se-$PbSe$-Sb_2Se_3 systems were also conducted using the classical EMF method with a liquid glycerol electrolyte.

For this purpose, concentration cells of the following type were constructed relative to the PbX (X = Se, Te) electrode:

(–) PbX (s) | liquid electrolyte, Pb^{2+}| $(2PbX)_x(AgSbX_2)_{1-x}$ (s)(+)

A solution of KCl in glycerol with added $PbCl_2$ was used as the electrolyte. EMF measurements were performed in the temperature range of 300–450 K.

The partial thermodynamic functions of PbX and Pb in alloys were calculated from the equations of the temperature dependences of the EMF. Potential-forming reactions were determined based on the diagrams of solid-phase equilibria in the Ag_2X-$A^{IV}X$-$B^{V}{}_2X_3$ systems. These reactions were used to calculate the standard thermodynamic functions of formation and the standard entropies of the $(2A^{IV}X)_x(AgB^{V}X_2)_{1-x}$ solid solutions, and a consistent set of data

on their standard partial and integral thermodynamic functions was obtained (Table 7).

Table 7.

Standard integral thermodynamic functions of solid solutions $2A^{IV}X$-$AgB^{V}X_2$ at 298 K [15, 25, 27, 38, 39]

Composition	$-\Delta_f G^0(298K)$	$-\Delta_f H^0(298K)$	$S^0(298K)$,
	кJ·mo^{-1}		J·K^{-1}·mol^{-1}
$(2SnTe)_{0,9}(AgSbTe_2)_{0,1}$	118.9±1.9	117.9±1.9	204.7±7.9
$(2SnTe)_{0,8}(AgSbTe_2)_{0,2}$	114.2±1.7	112.3±1.8	206.3±7.3
$(2SnTe)_{0,6}(AgSbTe_2)_{0,4}$	102.6±1.4	99.9±1.5	206.8±6.2
$(2SnTe)_{0,4}(AgSbTe_2)_{0,6}$	87.8±1.1	86.7±1.2	204.7±5.1
$(2SnTe)_{0,2}(AgSbTe_2)_{0,8}$	75.9±0.8	72.9±0.9	202.3±3.8
$(2SnTe)_{0,9}(AgBiTe_2)_{0,1}$	120.1±1.9	119.2±1.9	200.8±8.1
$(2SnTe)_{0,8}(AgBiTe_2)_{0,2}$	116.5±1.8	115.0±1.8	198.5±7.9
$(2SnTe)_{0,6}(AgBiTe_2)_{0,4}$	108.6±1.6	105.9±1.5	193.1±7.3
$(2SnTe)_{0,4}(AgBiTe_2)_{0,6}$	98.8±1.4	95.5±1.3	186.0±6.8
$(2SnTe)_{0,2}(AgBiTe_2)_{0,8}$	88.4±1.1	84.4±1.1	176.8±6.4
$(2PbSe)_{0.1}(AgSbSe_2)_{0.9}$	103.3±4.8*	102.2±5.1*	183.0±6.0*
$(2PbSe)_{0.2}(AgSbSe_2)_{0.8}$	114.3±5.0*	113.6±5.0*	185.2±5.5*
$(2PbSe)_{0.4}(AgSbSe_2)_{0.6}$	136.8±5.3*	136.6±4.8*	189.0±4.8*
$(2PbSe)_{0.6}(AgSbSe_2)_{0.4}$	158.2±5.6*	159.1±4.6*	190.9±4.0*
$(2PbTe)_{0,9}(AgSbTe_2)_{0,1}$	128.5±2.8	130.0±1.2	217.6±4.1
$(2PbTe)_{0,8}(AgSbTe_2)_{0,2}$	119.0±2.5	121.9±1.1	218.4±3.9
	122.2±2.9*	122.3±2.5*	220.0±3.5*
$(2PbTe)_{0,6}(AgSbTe_2)_{0,4}$	104.3±2.0	104.2±0.9	213.7±3.4
	106.4±2.3*	105.2±2.0*	216.1±3.5*
$(2PbTe)_{0,4}(AgSbTe_2)_{0,6}$	86.3±1.6	85.4±0.9	208.2±3.5
	89.1±1.8*	86.8±1.5*	211.5±3.8*
$(2PbTe)_{0,2}(AgSbTe_2)_{0,8}$	67.3±1.1	66.0±0.7	202.2±3.0
	69.8±1.2*	67.0±0.9*	204.9±3.7*

** These values were obtained using the EMF method with a liquid electrolyte*

From Table 7, it can be seen that the standard thermodynamic functions of formation and standard entropies for the studied solid solutions of the $2PbTe$-$AgSbTe_2$ system, obtained by two modifications of the EDS method, agree with each other within the

error limits.

Thus, as a result of systematic research conducted in this dissertation, new, consistent data were obtained on the phase equilibria, thermodynamic, and crystallographic properties of several ternary and quaternary systems based on copper (silver) and arsenic (antimony) chalcogenides. The resulting data sets form the physicochemical basis for the development of environmentally friendly functional materials for modern high technologies.

MAIN RESULTS AND CONCLUSIONS

1. Using traditional methods of physicochemical analysis (DTA, X-ray diffraction, SEM, microhardness measurements) and two modifications of the EMF method (concentration relative to the electrodes of galvanic cells with Cu^+ (Ag^+) cation-conducting solid electrolytes ($Cu_4RbI_3Cl_2$ and Ag_4RbI_5) and with a glycerol electrolyte, complexes of new mutually consistent data on phase equilibria in ternary Cu(Ag)-As(Sb)-S(Se) and quasi-ternary Ag_2X-$A^{IV}X$-$B^V{}_2X_3$ (A^{IV}-Sn, Pb; B^V-Sb, Bi; X – Se, Te) systems and the thermodynamic properties of the intermediate phases formed in them were obtained [1, 6, 10, 21, 35, 38, 41, 42, 45, 47, 52].
2. New refined pictures of phase equilibria in the ternary systems Cu-As-S, Cu-As-Se, and Cu-Sb-S were obtained, for which incomplete and contradictory data were available in the literature. Projections of the liquidus surface, diagrams of solid-phase equilibria at 300 K, and a number of polythermal sections of T-x-y phase diagrams were constructed. The fields of primary crystallization of phases, types, and coordinates of invariant and monovariant equilibrium reactions in each system were determined. It was shown that in sulfide systems, sections of the Cu_2X-$B^V{}_2S_3$ type, in contrast to the available data, are unstable in certain composition ranges, and this greatly affects the nature of phase equilibria in the ternary system as a whole [41, 45, 47, 52].
3. The existence of the following thermodynamically stable ternary compounds has been established in the Cu-As-S(Se) and Cu-Sb-S systems: Cu_3AsS_4, $Cu_{12}As_4S_{13}$, $Cu_6As_4S_9$, and CuAsS in the Cu-

As-S system; Cu_3AsSe_4, Cu_3AsSe_3, $Cu_7As_6Se_{13}$, $CuAsSe_2$, and CuAsSe in the Cu-As-Se system; CuSbS2, Cu_3AsSe_4, Cu_3AsSe_3, $Cu_7As_6Se_{13}$, $CuAsSe_2$, and CuAsSe in the Cu-Sb-S system. Other ternary compounds (Cu_5AsS_4, Cu_3AsS_3, $Cu_4As_2S_5$, $Cu_6As_4Se_9$, $Cu_4As_2Se_5$, etc.), previously mentioned in the literature, are most likely metastable phases. All stable compounds were obtained in a single-phase state, their crystallographic parameters, character, and melting temperatures were determined [41, 45, 47, 52].

4. The nature of the physicochemical interaction in the Ag_2Te-SnTe-Sb_2Te_3, Ag_2Te-SnTe-Bi_2Te_3, Ag_2Se-PbSe-Sb_2Se_3, and Ag_2Te-PbTe-Bi_2Te_3 systems was established for the first time. It was shown that they are stable planes of the corresponding quaternary systems and are characterized by the formation of continuous or wide regions of substitutional solid solutions along sections of the $A^{IV}X$-$AgB^{V}X_2$ type. For all of the aforementioned quasi-ternary systems, projections of the liquidus surfaces onto the concentration triangle, some isothermal sections, including room temperature, and a number of vertical sections of volume phase diagrams were constructed. Non- and monovariant equilibria were determined at the points and curves delimiting the fields of primary crystallization of the phases [21, 22, 29, 35, 38].
5. Various polythermal sections of the T-x-y phase diagrams of the studied quasi-ternary systems and some composition-property diagrams were constructed, and the homogeneity regions of the solid solutions formed in them were determined. It was shown that they have the form of wide bands, significantly (up to 8-10 mol%) extending beyond the $A^{IV}X$-$AgB^{V}X_2$ section line in both directions. These data are extremely important for the rational selection of solid solution compositions, which are of great interest as low-thermal-conductivity thermoelectric materials, known as LAST alloys, for physical measurements [21, 22, 29, 35, 38].
6. The nature of phase equilibria in the Cu–Ge–Sb–X (X = S, Se) systems was determined for the Cu_3SbS_4–GeS_2 and Cu_3SbSe_4–$GeSe_2$ sections. In both systems, solid solutions based on the initial ternary compounds with Sb→Ge substitution up to 15

mol.% were identified [40, 43, 44].

7. The concentration-temperature dependences of the EMF of electrochemical cells with a solid $Cu^{+}(Ag^{+})$-conducting electrolyte were established for all studied systems, and for the $Ag_2Se(Te)$-$PbSe(Te)$-$Sb_2Se_3(Te_3)$ systems, also for cells with a liquid glycerol electrolyte. It was shown that the nature of these dependences is consistent with the solid-phase equilibria diagrams. In particular, the temperature dependences of EMF are linear in the temperature range of measurements (300-380 K - sulfide systems and 300-450 K - selenide and telluride systems), which made it possible to use EMF data for thermodynamic calculations [1, 6, 10, 15, 21, 22, 25, 27, 28, 34, 38, 39, 41, 42, 47, 48, 52].
8. Based on the EMF measurements, the relative partial thermodynamic functions of copper (silver) or PbSe (Pb) in the alloys of the studied systems were calculated. Analysis of the isotherms of these functions showed that all three partial-molar functions within the homogeneity regions of the solid solutions are continuous functions of the composition and increase as the concentration of the potential-forming component decreases. This is consistent with the phase diagrams of the studied systems and the principles of solution thermodynamics. [1, 6, 10, 15, 21, 22, 25, 27, 28, 34, 38, 39, 41, 42, 47, 48, 52].
9. Using solid-phase equilibria diagrams of the studied ternary and quasi-ternary systems, virtual potential-forming reactions "occurring" in concentration electrochemical cells were determined, and standard thermodynamic formation functions ($\Delta_fG°$, $\Delta_fH°$), and standard entropies (S^0) of ternary compounds, as well as a number of selected compositions of $A^{IV}X$-$AgB^{V}X_2$ solid solutions, were calculated. The resulting sets of standard integral thermodynamic quantities have a high accuracy within the capabilities of the EMF method and are characterized by both internal consistency and consistency with the phase diagrams of the corresponding systems [15, 21, 22, 25, 27, 38, 39].
10. Based on the analysis of the obtained data sets on phase

equilibria and thermodynamic properties of the studied systems and available literature data on related systems, some features of phase formation and phase equilibria in them are noted [34, 49].

THE MAIN RESULTS OF THE DISSERTATION WORK ARE PUBLISHED IN THE FOLLOWING WORKS:

1. Babanly, M.B. Thermodynamic study of the Ag-As-Se and Ag-S-I systems using the EMF method with a solid Ag_4RbI_5 electrolyte / M.B. Babanly, L.F. Mashadieva, G.M. Velieva [et al.] // **Russian Journal of Electrochemistry**, - Moscow: 2009. vol.45, - p. 399–404. (Web of Science)
2. Юсибов, Ю.А., Алвердиев, И.Дж., Машадиева, Л.Ф., Бабанлы, М.Б. Твердофазные равновесия в системах Ag_2X-Sb_2X_3-X (X-Se, Te) и термодинамические свойства промежуточных фаз // "Biokimyəvi nəzəriyyələrin aktual problemləri" 2-ci Beynəlxalq Konfrans, - Gəncə, - 2011, - c. 126-131.
3. Бабанлы, М.Б., Алиев, И.И., Адыгезалова, З.В., Машадиева, Л.Ф. Фазовые равновесия в системе Ag_2Te-SnTe-Bi_2Te_3 // XIV всероссийская конференция "Высокочистые вещества и материалы. Получение, анализ применение", - Нижний Новгород, - 2011, - с. 184.
4. Бабанлы, М.Б., Машадиева, Л.Ф., Адыгезалова, З.В., Юсибов, Ю.А. Термодинамическое исследование систем Ag-Sb-Se(Te) методом ЭДС с твердым электролитом Ag_4RbI_5 // VI Украинский съезд по электрохимии. Днепропетровск, - 2011, - с. 175-179.
5. Бабанлы, Н.Б., Юсибов, Ю.А., Гасанова, З.Т., Машадиева, Л.Ф., Бабанлы, М.Б. Термодинамическое исследование сульфидов меди с p^3-элементами методом ЭДС с твердым электролитом // II Международная научно-техническая конференция “Функциональные и конструкционные материалы”, - Донецк, - 2011, - с. 23.
6. Babanly, M.B. Thermodynamic study of the Cu-As-S system by EMF measurements with $Cu_4RbCl_3I_2$ as a solid electrolyte / M.B.Babanly, Z.T.Gasanova, L.F.Mashadieva [et al.] // **Inorganic Materials**, - Moscow: 2012. vol.48, - p. 225–228. (Web of Science)
7. Mashadiyeva, L.F., Mansimova, Sh.H., Babanly, M.B. Phase

equilibria in Ag_2Se-PbSe-Sb_2Se_3 system and some properties of intermediate phases // XII International conference on crystal chemistry of intermetallic compounds. Lviv, Ukraine, - 2013, - p. 79.
8. Машадиева, Л.Ф., Мансимова, Ш.Г., Байрамов, В.Э., Юсибов, Ю.А., Бабанлы, М.Б. Исследование растворимости и термодинамических свойств твердых растворов в системах Sn(Pb)Te-$AgSbTe_2$ методом ЭДС с твердым электролитом Ag_4RbI_5 // XVI Российская конференция по физической химии и электрохимии расплавленных и твердых электролитов. Екатеринбург, Russia, - 2013, - с. 135.
9. Бабанлы, М.Б., Машадиева, Л.Ф., Кевсер, Дж., Мансимова, Ш.Г., Алиев, И.И. Термодинамическое исследование систем Ag_2Te-Sn(Pb)Te-Sb_2Te_3 методом ЭДС с твердым электролитом Ag_4RbI_5 // V международная конференция «Современные методы в теоретической и экспериментальной электрохимии», - Плес, Ивановская область, - 2013, - с. 73
10. Gasanova, Z.T. Thermodynamic study of the Ag_2S-As_2S_3-S system by EMF measurements with Ag_4RbI_5 as a solid electrolyte / Z.T.Gasanova, L.F.Mashadieva, V.P.Zlomanov [et al.] // **Inorganic Materials**, - Moscow: - 2014. vol.50, - p. 6–9 (Web of Science)
11. Бабанлы, Н.Б., Кевсер, Дж., Машадиева, Л.Ф., Джафаров, Я.И., Алиев, И.И. Поверхности первичной кристаллизации фаз в квазитройных системах Ag_2Te-Sn(Pb)Te-Bi_2Te_3 // VIII Международная научная конференция "Кинетика и механизм кристаллизации. Кристаллизация как форма самоорганизации вещества", - Иваново: - 2014, - с. 153-154.
12. Гасанова, З.Т., Машадиева, Л.Ф., Кулиева, У.А., Бабанлы, М.Б. Фазовая диаграмма системы Cu_2S-Cu_3AsS_4-S // XV Всероссийская конференция "Высокочистые вещества и материалы. получение, анализ, применение", - Нижний Новгород, Россия: - 2015, - с. 103.
13. Гасанова, З.Т., Машадиева, Л.Ф., Мирзоева, Р.Дж., Бабанлы, М.Б. Поверхность ликвидуса системы Cu_2Se-Cu_3AsSe_4-Se // VII Всероссийская конференция "физико-химические процессы в конденсированных средах и на межфазных границах- ФАГРАН-2015", - Воронеж, - 2015, - с. 331-332.
14. Гасанова, З.Т., Машадиева, Л.Ф., Мирзоева, Р.Дж., Бабанлы,

М.Б. Физико-химическое взаимодействие Cu_3AsSe_4 с селенидами меди // Akademik T.N.Şaxtantinskinin 90 illik yubileyinə həsr olunmuş respublika elmi konfransı, - Bakı, - 2015, - s. 117.
15. Кевсер, Дж. Термодинамические свойства твердых растворов в системе $2SnTe-AgBiTe_2$ / Дж. Кевсер, Л.Ф. Машадиева, А.Н. Мамедов [et al.] // Международный журнал прикладных и фундаментальных исследований, - Penza: - 2016. 3(7), - с. 404-407.
16. Mashadiyeva, L.F., Mansimova, Sh.H., Yusibov, Y.A., Babanly, M.B. New variable composition phases in the Ag-Pb-Sb-Se (Te) systems // 2nd International Turkic World Conference on Chemical Sciences and Technologies, - Skopje, - 2016, - p. 243.
17. Мансимова, Ш.Г., Машадиева, Л.Ф., Ильяслы, Т.М., Бабанлы, М.Б. Фазовая диаграмма системы $Ag_2Se-PbSe-Sb_2Se_3$ и некоторые свойства твердых растворов // XI международное Курнаковское совещание по физико-химическому анализу, - Воронеж, - 2016, - с. 162-163.
18. Mashadiyeva, L.F., Mansimova, S.Q., Veliyeva, G.M., Babanly, M.B. Thermodynamic study of the $PbSe-AgSbSe_2$ solid solutions using EMF method with solid-state electrolyte Ag_4RbI_5 // 13-го Совещания с международным участием "Фундаментальные проблемы ионики твердого тела", - Черноголовка, - 2016, - с. 496-497.
19. Гасанова, З.Т, Машадиева, Л.Ф, Мирзоева, Р.Дж, Бабанлы, М.Б. T-x-y диаграмма системы Cu-As-Se в области составов $Cu_2Se-Cu_3AsSe_4-Se$ // AMEA-nın akad.M.Nağıyev ad. Kataliz və Qeyri-üzvi Kimya İnstitutunun 80 illik yubileyinə həsr olunmuş elmi konfransı, - Баку, - 2016, - с. 43.
20. Машадиева, Л.Ф., Кевсер, Дж., Бабанлы, К.Н., Алиев, И.И., Юсибов, Ю.А. Твердофазные равновесия в системе $Ag_2Te-SnTe-Sb_2Te_3$ и термодинамические свойства твердых растворов // Всероссийская конференция «Химия твердого тела и функциональные материалы - 2016», - Екатеринбург, - 2016, - с. 230-231.
21. Mashadiyeva, L.F. The $Ag_2Te-SnTe-Bi_2Te_3$ system and thermodynamic properties of the $(2SnTe)_{1-x}(AgBiTe_2)_x$ solid solutions series / L.F. Mashadiyeva, J.O. Kevser, I.I. Aliev [et al.] // **Journal of Alloys and Compounds**, - Amsterdam: - 2017. vol.724, - p. 641-648. (Web of Science)

22. Mashadiyeva, L.F. Phase equilibria in the Ag_2Te-$SnTe$-Sb_2Te_3 system and thermodynamic properties of the $(2SnTe)_{12x}(AgSbTe_2)_x$ solid solution / L.F.Mashadiyeva, J.O.Kevser, I.I.Aliev [et al.] // **Phase equilibria and diffusion**, - Amsterdam: - 2017. 38(5), - p. 603-614. (Web of Science)
23. Gasanova, Z.T. Phase equilibria in the Cu_2S–Cu_3AsS_4–S system / Z.T. Gasanova, L.F. Mashadieva, Y.A. Yusibov [et al.] // **Russian Journal Inorganic Chemistry**, - Moscow: - 2017. vol.62, - p. 591–597 (Web of Science)
24. Mashadieva, L.F. Phase equilibria in the Cu–Cu_2Se–As system / L.F. Mashadieva, , Z.T. Gasanova, Y.A. Yusibov [et al.] // **Russian Journal Inorganic Chemistry**, - Moscow: - 2017. vol. 62, - p. 598–603 (Web of Science)
25. Mashadieva, L.F. Thermodynamic Study of Solid Solutions in the SnTe–$AgSbTe_2$ System by Means of EMF with Solid Electrolyte Ag_4RbI_5 / L.F.Mashadieva, Y.A.Yusibov, Dzh.Kevser // **Russian Journal of Physical Chemistry A**, - Moscow: - 2017. 91(9), - p. 1642–1646 (Web of Science)
26. Mashadiyeva, L.F., Mansimova, Sh.H., Kevser, J.O., Yusibov, Yu.A., Babanly, M.B. Thermodynamic study of the $A^{IV}Te$-$AgSbTe_2$ (A^{IV}-Sn, Pb) systems by EMF technique // "3rd International Turkic World Conference on Chemical Sciences and Technologies (ITWCCST 2017)'', - Baku, Azerbaijan: - 2017, - p. 303.
27. Mashadieva, L.F. Thermodynamic study of the $2PbTe$–$AgSbTe_2$ system using EMF technique with the Ag_4RbI_5 solid electrolyte / L.F. Mashadieva, Sh.G. Mansimova, Yu.A. Yusibov // **Russian Journal of Electrochemistry**, - Moscow: - 2018. 54 (1), - p. 106–111 (Web of Science)
28. Mashadieva, L.F. Phase equilibria in the Cu_2Se–Cu_3AsSe_4–Se system and thermodynamic properties of Cu_3AsSe_4 / L.F. Mashadieva, Z.T. Gasanova, Yu.A. Yusibov // **Inorganic Materials**, - Moscow: - 2018. 54(1), - p. 8–16. (Web of Science)
29. Mansimova, S.H. Phase equilibria in the PbSe-$AgSbSe_2$ system / S.H. Mansimova, K.N. Babanly, L.F. Mashadiyeva // **Chemical Problems**, - Baku: - 2018. №4, - p. 530-536. (Scopus)
30. Мансимова, Ш.Г., Машадиева, Л.Ф., Юсибов, Ю.А., Бабанлы, М.Б. Взаимная растворимость и термодинамические свойства твердых растворов в системе $2PbSe$-$AgSbSe_2$ // Всероссийская конференция С

международным участием "Химия твердого тела и функциональные материалы" и XII всерлссийский симпозиум с межд. участием "Термодинамика и материаловедение", - Санкт-Петербург, - 2018, - с. 264.
31. Мансимова, Ш.Г., Машадиева, Л.Ф., Буланова, М.В., Бабанлы, М.Б. Новые фазы переменного состава в системе PbSe-$AgSbSe_2$. // "Müasir təbiət və iqtisad elmlərinin aktual problemləri" beynəlxalq konfrans, - Gəncə, - 2018, - s. 100-101.
32. Гасанова, З.Т., Машадиева, Л.Ф., Кулиева, У.А., Бабанлы, М.Б. Фазовая диаграмма системы Cu_2S-Cu_3AsS_4-S // "Высокочистые вещества и материалы. Получение, анализ, применение" XVI всероссийская конф. и IX школа молодых ученых, посв. 100-летию Г.Г.Девятых, – Новгород, - 2018, - с. 43.
33. Мансимова, Ш.Г., Машадиева, Л.Ф., Бабанлы, К.Н., Юсибов, Ю.А. Твердофазные равновесия в системе Ag_2Te-PbTe-Sb_2Te_3 и некоторые свойства твердых растворов // VIII Всероссийская конференция "Физико-химические процессы в конденсированных средах и на межфазных границах-ФАГРАН-2018", - Воронеж, Россия: - 2018, - с. 434-435.
34. Babanly, M.B. Some issues of complex investigation of the phase equilibria and thermodynamic properties of the ternary chalcogenide systems by the EMF method / M.B.Babanly, L.F.Mashadiyeva, D.M.Babanly [et al.] // **Russian Journal of Inorganic Chemistry**, - Moscow: - 2019. 64(13), - p. 1649-1671. (REVIEW) (Web of Science)
35. Mansimova, Sh.H. Phase Equilibria In The Ag_2Se-PbSe-$AgSbSe_2$ system / Sh.H.Mansimova, K.N.Babanly, L.F.Mashadiyeva [et al.] // **Chemical Problems**, - Baku: - 2019. 17(1), - p. 41-49. (Scopus)
36. Əşirov, G.M., Məşədiyeva, L.F., Həsənova, Z.T., Əmiraslanov, İ.R., Babanlı, M.B. Cu_2S-Sb_2S_3 sistemində faza tarazlıqları // Müasir təbiət və iqtisad elmlərinin aktual problemləri, - Gəncə, - 2019, - s. 10-13.
37. Mashadiyeva, L.F., Mansimova, Sh.H., Babanly, D.M., Shukurova, G.M., Babanly, M.B. Thermodynamic investigation of the PbX-$AgSbX_2$ (X-Se, Te) systems using two modifications of the emf method // XXII International Conference on Chemical Thermodynamics in Russia, - Saint-Petersburg, Russia: - 2019, - p. 204.

38. Mashadiyeva, L.F. Phase equilibria in the Ag_2Te-$PbTe$-Sb_2Te_3 system and thermodynamic properties of the $(2PbTe)_{1-x}(AgSbTe_2)_x$ solid solutions / L.F. Mashadiyeva, S.H. Mansimova, D.M. Babanly // **Acta Chimica Slovenica**, - Ljubljana: - 2020. vol.67, - p. 799–811. (Web of Science)
39. Mashadiyeva, L.F. Thermodynamic properties of solid solutions in the PbSe—$AgSbSe_2$ system / L.F. Mashadiyeva, Sh.G. Mansimova, K.N. Babanly // **Russian Chemical Bulletin**, - Nyu York: - 2020. 69(4), - p. 660–664. (Web of Science)
40. Ismailova, E.N., Hasanova, Z.T., Babanly, K.N., Mashadiyeva, L.F. Solid solutions based on Cu_3SbSe_4 in the Cu_3SbSe_4-$SnSe_2$ ($GeSe_2$) systems // 9th Rostocker International Conference: "Technical Thermodynamics: Thermophysical Properties and Energy Systems" THERMAM 2020, Book of Abstracts, - Rostock, - 2020, - p. 84.
41. Mashadiyeva, L.F. Solid-phase equilibria in the Cu-Sb-S system and thermodynamic properties of copper-antimony sulphides / L.F. Mashadiyeva, P.R. Mammadli, D.M. Babanly // **Journal of minerals, Metals & Materials Society (JOM)**, - Pittsburgh: - 2021. 73(5), - p. 1522-1530 (Web of Science)
42. Mashadieva, L.F. Thermodynamic study of the Ag–Sb–Se system by the EMF method with Ag_4RbI_5 solid electrolyte / L.F. Mashadieva, D.M. Babanly, Yu.A. Yusibov // **Russian Journal of Electrochemistry**, - Moscow: - 2021. 57(3), - p. 281–288 (Web of Science)
43. Ismayilova, E.N. Phase equilibria along the Cu_3SbSe_4-$GeSe_2$ section of the Cu-Ge-Sb-Se system / E.N. Ismayilova, A.N. Baladzhayeva, L.F. Mashadiyeva // **New Materials, Compounds and Applications**, - Baku: - 2021. 5(1), - p. 52-58 (Web of Science)
44. Баладжаева, А.Н., Исмайлова, Э.N., Шевельков, А.В. Фазовые равновесия по разрезу Cu_3SbS_4-GeS_2 системы Cu-Ge-Sb-S // "Müasir təbiət və iqtisad elmlərinin aktual problemləri" Beynəlxalq elmi konfrans, - Gəncə, - 2021,- s. 42-45
45. Mashadiyeva, L.F. Liquidus surface and phase relations in the Cu-Sb-S system // Capter II in Book: Properties and Uses of Antimony – Editor: David J. Jenkins / L.F.Mashadiyeva, D.M.Babanly, A.N.Poladova [et al.] // Nova Science Publishers, - New York: - 2022. - p. 45-72. (Scopus)

46. Mashadiyeva, L.F., Babanly, D.M., Yusibov, Yu.A., Babanly, M.B. Thermodynamic investigation of copper and arsenic selenides by the emf method with the $Cu_4RbCl_3I_2$ solid electrolyte // 16th International Meeting «Fundamental Problems of Solid State Ionics», - Moscow, - 2022, - p. 419.
47. Mashadiyeva, L.F. Phase relations in the Cu-As-S system and thermodynamic properties of copper-arsenic sulfides / L.F. Mashadiyeva, D.M. Babanly, Z.T. Hasanova // **Journal of Phase Equilibria and Diffusion**, - New York: - 2024. vol. 45, - p. 567–582. (Web of Science)
48. Babanly, M.B. Thermodynamic properties of complex copper chalcogenides / M.B. Babanly, L.F. Mashadiyeva, S.Z. Imamaliyeva // **Chemical Problems**, - Baku: - 2024. 22(3), - p. 243-280. (REVIEW) (Scopus)
49. Babanly, M.B. Complex copper-based chalcogenides: a review of phase equilibria and thermodynamic properties / M.B. Babanly, L.F. Mashadieva, S.Z. Imamaliyeva // **Condensed Matter and Interphases**, - Voronej: - 2024. 26(4), - p. 579-619 (REVIEW) (Scopus)
50. Mashadiyeva, L.F. Phase equilibria in the Cu_2Se-Cu_3AsSe_4-As_2Se_3 system / L.F. Mashadiyeva, Z.T. Hasanova, Yu.A. Yusibov // **Azerbaijan Chemical Journal**, - Baku: - 2024. № 3, - p. 83-93. (Scopus)
51. Юсибов, Ю.А., Машадиева, Л.Ф., Гасанова, З.Т., Бабанлы, М.Б. Уточнение фазовой диаграммы системы Cu_2Se-As_2Se_3 // Ümummilli lider H.Əliyevin anadan olmasının 101 illiyinə həsr olunmuş "Müasir təbiət və iqtisad elmlərinin aktual problemləri" beynəlxalq konfrans, - Gəncə, - 2024, - s. 12-15.
52. Mashadiyeva, L.F. New picture of phase equilibria in the Cu-As-Se system and thermodynamic properties of ternary compounds / L.F. Mashadiyeva, A.N. Poladova, Z.T. Hasanova // **Chemical Problems**, - Baku: - 2025. 23(3), - p. 310-328. (Scopus)

The defense will be held on 30 October 2025 at $10^{\underline{00}}$ at the meeting of the Dissertation council ED1.15 of Supreme Attestation Commission under the President of the Republic of Azerbaijan operating at Institute of Catalysis and Inorganic Chemistry named after acad.M.Naghiyev of the Ministry of Science and Education of the Republic of Azerbaijan

Address: H.Javid Avenue, 113, AZ-1073, Baku, Azerbaijan

The dissertation is accessible at the library of the Institute of Catalysis and Inorganic Chemistry named after acad. M.Naghiyev of the Ministry of Science and Education of the Republic of Azerbaijan

Electronic versions of dissertation and its abstract are available on the official website of the Institute of Catalysis and Inorganic Chemistry named after acad.M.Naghiyev of the Ministry of Science and Education of the Republic of Azerbaijan www.kqkiamea.az

Abstract was sent to the required addresses on 29 September 2025

Signed for printing: 25.09.2025

Paper format: 60x84$^{1/16}$

Volume: 77 169 characters

Number of hard copies: 20